Age-related declines in niche self-renewal factors controls testis aging and spermatogonial stem cell competition through Hairless, Imp, and Chinmo

Yu Zheng[1†], Ya-Chien Lee[1†], Yu-Ting Wang[2, 3], Pin-Kuan Chiang[1], Shao-Lun Chang[1], Hwei-Jan Hsu[2, 3], Li-Sung Hsu[6], Erika A. Bach[4, 5]*, Chen-Yuan Tseng[1]*

Affiliations

[1] Institute of Molecular Biology, National Chung-Hsing University, Taichung, Taiwan.

[2] Graduate Institute of Life Science, National Defense Medical Center, Taipei, Taiwan.

[3] Institute of Cellular and Organismic Biology, Taipei, Taiwan.

[4] Department of Biochemistry and Molecular Pharmacology,

[5] Helen L. and Martin S. Kimmel Center for Stem Cell Biology, NYU Grossman School of Medicine, New York, NY 10016, USA

[6] Institute of Medicine, Chung Shan Medical University, Taichung, Taiwan.

[†]equal contribution

[*]Corresponding authors erika.bach@nyu.edu and chenyuan1102@dragon.nchu.edu.tw

Highlights

- Aged niche cells produce less BMPs, resulting in more Hairless (H) in aged GSCs
- Elevated H represses *Imp*, resulting in less Chinmo and in ectopic ECM secretion
- Aging is prevented by higher BMP in niche cells, or by higher Imp or lower H in GSCs
- GSCs with low *Imp* or high *H* exploit these aging mechanisms to colonize the GSC pool

Summary

Aging is associated with progressive tissue decline and shifts in stem cell clonality. The role of niche signals in driving these processes remains poorly understood. Using the *Drosophila* testis, we identify a regulatory axis in which age-related decline of niche signals (BMPs) lead to upregulation of the co-repressor Hairless, which downregulates the RNA-binding protein Imp in aged germline stem cells (GSCs). Reduced Imp causes loss of Chinmo, a key factor in GSC aging and competition. Reduced Chinmo causes ectopic Perlecan secretion which accumulates in the testis lumen and causes GSC loss. Aging of the testis is reversed by increasing BMPs in the niche, or by overexpressing Imp or depleting Hairless in GSCs. Furthermore, GSC clones with reduced Imp or increased Hairless are more competitive, expelling wild-type neighbors and monopolizing the niche. Thus, BMPs regulate testicular niche aging through the Hairless–Imp–Chinmo axis and "winning" GSCs usurp these aging mechanisms.

Keywords

BMP; Dpp; Gbb; Hairless; Imp; Chinmo; stem cell niche; spermatogonial stem cell; germline stem cell; *Drosophila*; testis; competition; aging

Introduction

Adult organs rely on tissue stem cells for lifelong maintenance. These stem cells typically reside in specialized microenvironments termed niches, which provide short-range signals essential for preserving stemness [1]. However, as organisms age, niche functionality declines, resulting changes in secretion of soluble factors and in biophysical properties of the

48 microenvironment [2]. The age-dependent decline in niche function reduces both stem cell activity
49 and overall stem cell numbers, leading to age-related organ dysfunction [2,3]. In humans, the
50 decline in fertility in older men is due in part to the dysfunction of Sertoli and Leydig cells—key
51 components of the spermatogonial stem cell (SSC) niche [4-9]. Mouse models similarly
52 demonstrate age-dependent reductions in fertility and testis function, driven by decreased
53 production of niche-derived signals such as glial cell-derived neurotrophic factor in older Sertoli
54 cells [10]. Consecutive transplantation of aged SSCs to the testes of young male mice maintains
55 stem cell function for extended periods of time as the result of younger niches [11].
56 Competition among adult stem cells often occurs with aging and results from extrinsic
57 and intrinsic events. The age-altered microenvironment can exert different selective forces on
58 resident stem cells, and stem cells can sustain age-dependent mutations that could impart a
59 selection advantage [12]. Stem cell competition is implicated in a range of human pathologies. A
60 well-known example is clonal hematopoiesis, where a small subset of hematopoietic stem cells
61 (HSCs) expands to dominate the population in approximately 10% of older adults, markedly
62 elevating the risk of leukemia [13,14]. Age-related shifts in stem cell clonality have been observed
63 in other adult somatic tissues and can underlie cancer risk [15-25]. In the male germline, paternal
64 age effect (PAE) disorders arise from *de novo* mutations in aging SSCs that confer a growth or
65 competitive advantage, leading to clonal expansion and an increased proportion of mutant cells
66 in the seminiferous tubules [26]. These "selfish" mutations pose serious risks to offspring [27].
67 Despite their clinical importance, *in vivo* models for PAE are limited, and the phenomenon of
68 stem cell competition in the germline remains less explored than in the soma [28]. How age-
69 dependent changes in the niche microenvironment intersect with stem cell competitiveness
70 remains largely uncharacterized.
71 The *Drosophila* testis has proven to be a powerful model for studying both SSC niche
72 aging and SSC competition [29-33]. Each testis houses a niche comprising approximately 12 post-
73 mitotic cells, which support 8–10 SSCs (termed germline stem cells (GSCs) in flies) (**Fig. 1A**) [34].
74 Niche cells produce the cytokine Upd, which activates the JAK/STAT pathway in GSCs and
75 promotes adhesion to the niche but not GSC self-renewal *per se* [35-38]. Niche cells produce less
76 Upd declines in aged testes, contributing to decreased JAK/STAT signaling in older GSCs [30,31].
77 Niche cells also produce Bone Morphogenetic Protein (BMP) ligands Decapentaplegic (Dpp)
78 and Glass bottom boat (Gbb), which have been shown to be *bona fide* GSC self-renewal cues

[36,39-41]. Whether BMPs decline during aging in the testis niche and whether such a decline impacts age-related phenotypes in the testis remains unknown.

We previously reported that levels of the transcription factor Chinmo in germline stem cells (GSCs) regulate aging of the testis stem cell niche [33]. During aging, GSCs exhibit a progressive and significant decline in Chinmo expression. As Chinmo levels decrease, expression of its target genes—including those encoding the secreted extracellular matrix (ECM) protein Perlecan (Pcan) and the ECM-binding protein Dystroglycan (Dg)—significantly increases. These age-dependent transcriptional changes drive: (1) the formation of an ECM structure around the niche, termed the "moat"; (2) a substantial accumulation of Dg at the GSC–niche interface; and (3) a marked reduction in the number of GSCs. Notably, maintaining robust Chinmo levels in GSCs during adulthood can rejuvenate the aging testis stem cell niche.

In the same study, we also found that GSC clones homozygous mutant for *chinmo* exhibit a striking competitive advantage over wild-type (WT) neighbors, ultimately monopolizing the entire germline and leading to biased transmission of the chinmo-mutant allele [33]. Mechanistically, this advantage stems from hijacking the aging-associated niche remodeling process: *chinmo*-mutant GSCs ectopically secrete Pcan into the testis lumen, promoting moat formation. The moat impairs the ability of neighboring WT GSCs to adhere to the niche, compromising their maintenance. Simultaneously, *chinmo*-null GSCs upregulate Dg, allowing them to anchor themselves more effectively within the remodeled niche. However, the upstream factors that regulate Chinmo expression during aging have remained unknown, limiting our understanding of both testis niche aging and GSC competition.

Here, we show that Chinmo mRNA levels in GSCs are positively regulated by the RNA-binding protein (RBP) IGF-II mRNA-binding protein (Imp). We find that *Imp* mRNA and protein levels are robust in young GSCs but decline significantly with age. Importantly, sustaining Imp expression during adulthood preserves Chinmo levels and prevents testis aging phenotypes. Further analyses reveal that *Imp* is transcriptionally downregulated by the co-repressor Hairless (H), as *Imp* mRNA levels increase when H is depleted in aged GSCs. Manipulating H levels in GSCs modulates aging: loss of H alleviates aging, whereas overexpression of H accelerates it. Notably, H expression in GSCs is itself repressed by Bone Morphogenetic Protein (BMP) signals, specifically Dpp and Gbb, secreted by the niche. As BMP production declines with age, H levels rise in GSCs, leading to reduced Imp and subsequently

110 Chinmo, ultimately driving ectopic Pcan secretion and niche remodeling. Thus, the age-
111 dependent decline of niche-derived BMP signals converges on the H–Imp–Chinmo axis to
112 regulate aging of the testis stem cell niche.
113 Finally, we demonstrate that GSC clones with lower Imp or higher H levels exhibit
114 enhanced competitiveness, displacing neighboring WT GSCs from the niche similarly to
115 chinmo-mutant GSCs. Our findings reveal that competitive GSCs exploit the age-dependent
116 intrinsic and extrinsic changes regulating Chinmo expression, leading to stem cell niche
117 disruption and eventual monoclonality of the GSC lineage.
118

119 **Results**

120 **Chinmo is post-transcriptionally regulated in GSCs during aging**

121 We previously reported that Chinmo protein in GSCs significantly declines during
122 adulthood (**Fig. 1B-D**) [33]. Four *chinmo* mRNA isoforms (*chinmo-RA,-RD,-RG,-RH*) encode a
123 604 amino acid (aa) protein, and two isoforms (*chinmo-RE* and *-RF*) encode 840 aa protein (**Fig.**
124 **1F**). We established that *chinmo* is not transcriptionally regulated in GSCs during aging (**Fig.**
125 **1E,** third and fourth bars). This assay is robust because germline depletion of *chinmo* using an
126 RNAi transgene targeting all isoforms and the GSC-specific driver *nos-Gal4* (*nos>chinmo-i*)
127 caused a significant decline in *chinmo* mRNA abundance compared to control *nos>lacZ* testes
128 (**Fig. 1E**, first and second bars), Thus, *chinmo* appears to be regulated post-transcriptionally in
129 GSCs.
130 To confirm this, we used hybridization chain reaction (HCR) fluorescence *in situ*
131 hybridization (FISH) to determine *chinmo* mRNA isoform expression patterns. We used three
132 probes: one for *chinmo-RA, -RD, -RG,* and *-RH*; a second for *chinmo-RE* and *-RF*; and a third for
133 *chinmo-RH* (**Fig. 1F**). We found that *chinmo-RA, -RD, -RG,* and *-RH* isoforms are robustly
134 expressed in GSCs from young 2-day-old (D2) males and decline significantly in GSCs from
135 aged 42-day-old (D42) males (**Fig. 1G-I**). *chinmo-RE* and *-RF* are moderately expressed in
136 GSCs regardless of age (**Fig. 1J-L**), while *chinmo-RH* is expressed at very low levels in GSCs
137 regardless of age (**Fig. 1M-O**). *chinmo-RH* is the only isoform known to be targeted by
138 microRNAs (miRs) (i.e., *mir-let7*) through its 6 kb extended *3'UTR* [42]. The fact that *chinmo-RH*
139 is not regulated by aging in GSCs suggests that miRNAs are not responsible for *chinmo*
140 transcript downregulation during aging. Indeed, Chinmo protein was not altered in GSCs

141 deficient in miRNA processing components *Dcr-1*, *AGO1* or *drosha* or in *mir-let7* (**Fig. S1A-C,**
142 **E-I**). Additionally, *AGO1*-mutant GSCs cannot be recovered at 14 days post-clone induction
143 (dpci) (**Fig. S1D** and **Table S1 #6**), as previously reported [43], indicating that they are
144 hypocompetitive. Finally, although Chinmo is a JAK/STAT target gene in other cells [44], STAT-
145 deficient GSCs still express Chinmo protein, indicating that Chinmo is not regulated by the
146 JAK/STAT in male GSCs (**Fig. S1J-M**). Taken together, these results indicate that in male GSCs
147 *chinmo-RA*, *-RD* and *-RG* are downregulated during aging through a process that does not
148 involve miRs.
149
150 **Imp is required for GSC homeostasis during aging by promoting Chinmo protein**
151 **expression**
152 The RBP Imp promotes Chinmo expression in neuroblast lineages and binds *chinmo-RD*
153 mRNA in S2 cells [45,46]. We found that *Imp* mRNA is significantly decreased both in number and
154 size of puncta in GSCs from aging D28 males compared to young D2 males (**Fig. 2A-D**). Imp-
155 specific antibodies and protein traps revealed that Imp is robustly expressed in GSCs in WT
156 young D2 males and significantly declines in GSCs from WT aged D42 males (**Fig. 2E-L** and
157 **S2A-C**). As expected, Imp levels in niche cells declined during aging (**Fig. 2A-C** and **S2A,**
158 **B, D, E**) [31]. To test whether sustained expression of Imp can augment Chinmo expression in aged
159 GSCs, we over-expressed Imp in GSCs throughout adulthood using *nos-Gal4*. Exogenous Imp
160 significantly increased Imp protein in aged GSCs but not in aged niche cells (**Fig. S2D-G**) and
161 significantly increased Chinmo protein in aged GSCs (**Fig. 2M-O**). Furthermore, depletion of
162 *Imp* using two validated RNAi lines (**Fig. S3A-D**), caused a significant decline in Chinmo
163 protein compared to age-matched controls (**Fig. S3E-H**). These results indicate that Imp
164 promotes Chinmo expression in GSCs during homeostasis. We previously showed that the
165 number of GSCs declines during adulthood and that GSC number in aged D42 males could be
166 significantly restored by over-expressing Chinmo in GSCs [33]. We now show that sustained Imp
167 expression in GSCs (*nos>Imp*) throughout adulthood also restored GSC numbers in aged males
168 (*nos>lacZ*) (**Fig. 2P**). By contrast, the depletion of Imp further reduced the total GSC number in
169 aged D42 males (**Fig. S3I**). These results show that Imp regulates the number of GSCs during
170 aging by promoting Chinmo expression.
171

172 **Imp regulates age-dependent niche remodeling via Chinmo**

173 Our prior work revealed that testes from aged D42 WT males had ectopic ECM
174 accumulation around the niche (**Fig. 3A, C, E**) and that GSCs in these aged testes upregulated
175 the ECM-binding protein Dg at the GSC-niche interface to remain in the altered niche (**Fig. 3F,**
176 **H**) [33]. We also demonstrated that the ectopic ECM and Dg in older testes were reversed by
177 sustained Chinmo expression in GSCs [33]. We now show that sustained Imp expression in GSCs
178 throughout adulthood significantly suppressed the ectopic ECM (**Fig. 3B, D, E**) and ectopic Dg
179 at the GSC-niche interface in aged testes (**Fig. 3G, H**).

180 To determine whether the age-dependent effects of Imp occurred through Chinmo, we
181 examined ECM deposition and Dg localization in GSCs that were depleted for *Imp* and that
182 over-expressed Chinmo. We reasoned that if Chinmo functioned downstream of Imp, then
183 sustained Chinmo will rescue the effects of Imp depletion. For this experiment, we chose a
184 reproductive middle age time point of 21 days (D21) because few testes from control males
185 (*nos>lacZ, lacZ*) have ectopic ECM in the testis lumen or ectopic Dg (**Fig. 3I, M, N, R**). Testes
186 from D21 males with GSC depletion of *chinmo* (*nos>lacZ, chinmo-i*) or GSC depletion of Imp
187 (*nos>Imp-i, lacZ*) have a significant increase in luminal ECM and in Dg at the GSC-niche
188 interface (**Fig. 3J, K, M, O, P, R**); they also have a significant drop in the number of GSCs (**Fig.**
189 **3S**). Concomitant over-expression of Chinmo and depletion of Imp significantly reduced the
190 ectopic ECM and Dg and significantly increased the average total number of GSCs (**Fig. 3L, M,**
191 **Q-S**). These results indicate that Imp prevents stem cell niche aging through Chinmo.

192

193 **H negatively regulates Imp in GSCs**

194 Our data indicate that aged GSCs have reduced *Imp* mRNA (**Fig. 2A-D**). Consistent with
195 this, factors known to regulate *Imp* expression in other tissues (i.e., miRNAs, the RBP Syncrip
196 (Syp), and Chinmo [31,45,46]) did not impact Imp levels in male GSCs (**Fig. S4**). To identify factors
197 that control *Imp* in GSCs, we performed an RNAi screen of transcriptional regulators known to
198 genetically interact with *Imp* per Flybase and to be expressed in early germ cells per Fly Cell
199 Atlas: the transcription factors Ets21C and p53, and the co-repressor H [47-50]. We depleted these
200 factors individually in GSCs during adulthood and examined Imp protein. Only germline
201 depletion of H using two independent RNAi lines significantly altered Imp protein in GSCs (**Fig.**

202 S5A-G). Since Imp protein levels increase upon germline H depletion, H is a negative regulator
203 of Imp expression in GSCs.
204
205 **H expression in GSCs increases during aging**
206 To assess whether H expression in GSCs is modulated during aging, we assessed the
207 activity of the *H* gene using the $H^{CR60128\text{-}TG4.1}$-GAL4 line crossed to *UAS-mCD8-GFP*, encoding
208 a membrane-tethered GFP. We monitored *H* expression in young D2 males and aging D28 males
209 because there is a significant decline in the average total number of GSCs in WT testes at D28
210 (Fig. 4H) [33]. GSCs from young testes have low *H* expression as indicated by low levels of
211 membrane GFP (Fig. 4A). By contrast, GSCs from D28 males have robust *H* expression (Fig.
212 4B) that was similar to the positive control of membrane GFP driven by *nos-Gal4* (Fig. 4C). We
213 also found a significant increase in *H* transcripts and in protein during aging (Fig. 4D-G).
214
215 ***Imp* is transcriptionally regulated by H in GSCs**
216 Our results demonstrate that Imp and H exhibit opposite expression patterns in adult male
217 GSCs. Since H can decrease transcription of target genes [51], we determined whether H could
218 downregulate *Imp* transcripts. *Imp* mRNA is detected in GSCs in D28 control testes and is
219 significantly increased in H-depleted GSCs at this time point (Fig. 4I-K, M, N). As expected,
220 *Imp* levels in niche cells across the two genotypes were unchanged at D28 (Fig. 4L). These data
221 indicate that H transcriptionally regulates *Imp* in GSCs during homeostasis.
222
223 **Self-renewal cues regulate aging of the testis stem cell niche**
224 Because niche-derived soluble factors can decline with age [31], we investigated whether
225 reduced levels of the BMPs Dpp and Gbb might underlie GSC aging. Dpp and Gbb are well-
226 established self-renewal cues for GSC maintenance [36,39-41], but their role in testis stem cell niche
227 aging is not known. While we observed robust expression of both proteins in the niche cells of
228 young D2 testes, their levels were significantly diminished in D28 testes (Fig. 5A–F). We next
229 asked whether maintaining high levels of these ligands during adulthood would suppress the age-
230 dependent increase in H in GSCs. We overexpressed *UAS* transgenes encoding either Dpp::GFP
231 or Gbb::GFP in niche cells with the niche-specific driver *upd-Gal4* and examined H::GFP in
232 GSCs at D14 and D28. In both *upd>Dpp::GFP* and *upd>Gbb::GFP* testes, H::GFP was

233 significantly reduced in GSCs compared to controls (**Fig. 5G-J**). We evaluated whether
234 sustained BMP levels in niche cells would mitigate aging phenotypes at D28. In *upd>Dpp::GFP*
235 and *upd>Gbb::GFP* testes at D28, Chinmo was significantly elevated in GSCs, while Dg was
236 significantly reduced (**Fig. 5K, L**). Additionally, Pcan accumulation around the niche was
237 substantially reduced, and there were significantly more GSCs compared relative to age-matched
238 controls (**Fig. 5M, N**). Taken together, these findings indicate that H levels in GSCs are
239 negatively regulated by niche-derived BMPs and that sustaining robust BMP expression in niche
240 cells prevents aging-phenotypes.
241
242 **H acts in GSCs to promote aging of the testis stem cell niche**
243 Since BMPs repress H expression in GSCs, we hypothesized that GSC depletion of H
244 would ameliorate age-dependent phenotypes of the testis stem cell niche. Consistent with this
245 model, GSC depletion of H for 28 days significantly increased Chinmo protein (**Fig. 6A-C**),
246 significantly decreased ectopic Pcan in the testis lumen and ectopic Dg at the GSC-niche
247 interface (**Fig. 6D-I**) and significantly restored the average total number of GSCs compared to
248 the aged-match control (**Fig. 6J**). Similar results were observed with another independent *H*-
249 RNAi line (**Fig. S5H-Q**). Furthermore, we found that H over-expression in GSCs accelerated
250 aging of the testis stem cell niche. Over-expression of H using three independent *UAS* lines
251 ($H^{EY03696} = H^{EY}$, $H^{EP-211} = H^{EP}$, $H^{GS11776} = H^{GS}$) in GSCs caused a significant decline in Imp and
252 Chinmo proteins, resulting in significantly more luminal Pcan and Dg at the GSC-niche
253 interface, and impaired GSC homeostasis (**Fig. 6K-W**). Thus, both loss and gain of function
254 experiments indicate that H levels in GSCs regulate aging of the testis stem cell niche.
255
256 **H functions independently of Notch (N) signaling in GSCs**
257 N target genes are repressed by a complex of co-repressors (H, Groucho and dCtBP) that
258 recruit the transcription factor Suppressor of Hairless (Su(H)) [51,52]. Although we observe low
259 levels of Su(H)::GFP in GSCs, we did not detect any N transcriptional activity in the adult testis
260 using established reporters, even when we depleted H from GSCs (**Fig. S6A-E, H-K**). As
261 expected, N activity was observed in polar cells of the *Drosophila* ovary, indicating the efficacy
262 of the N reporters in adult gonads (**Fig. S6F, G**) [53]. Furthermore, ectopic activation of N using
263 the dominant-active NICD transgene in GSCs for 28 days of adulthood did not alter Imp protein

264 levels or the average total number of GSCs (Fig. S6L-O), which is consistent with our model
265 that H has N-independent functions in male GSCs (Fig. S6P).
266
267 ***Imp*-deficient or H-overexpressing GSC clones dominate their niche by evicting non-**
268 **mutant neighbors**
269 We previously demonstrated that *chinmo*-mutant GSC clones had a competitive
270 advantage over their non-mutant sibling GSCs by co-opting an aging mechanism (decline of
271 Chinmo protein in GSCs during aging) [33]. Next, we wanted to test whether *Imp*-mutant or H-
272 over-expressing GSC clones exhibit similar behavior. *Imp* is located on the X chromosome and
273 *Imp* mutations are lethal in males, precluding mosaic analysis. Instead, we induced MARCM
274 GSC clones that over-expressed a validated *Imp-RNAi* transgene and GFP or control clones that
275 expressed GFP [54]. We also employed the GSC-specific *nos* flip-out methodology (*nos-FRT-*
276 *STOP-SV40-polyA-FRT-gal4-VP16-nos 3'UTR*) [55] to generate *Imp*-mutant GSCs clones with a
277 second validated RNAi transgene and or H-overexpressing clones with two independent *UAS*
278 lines H^{EP} and H^{GS} (Fig. 7A). In both MARCM and *nos* flip-out techniques, the clones are GFP-
279 positive and the non-mutant sibling GSCs are GFP-negative (Figs. 7B-E; S7A,B). As expected,
280 *Imp-i* and H-overexpressing GSC clones have significantly lower Imp and Chinmo protein (Figs.
281 7E, F, L, M) and significantly increased ECM in the testis lumen (Figs. 7G-K, O; S7C-E) at 14
282 dpci compared to control clones. Additionally, H-overexpressing GSC clones have significantly
283 higher Dg at the GSC-niche interface compared to control clones (Fig. 7N).
284 To examine GSC competitiveness, we quantified the percent of *Imp-i* and H-over-
285 expressing clones composing the GSC pool, termed "clone occupancy" [33], at 2 and 14 dpci (Fig.
286 7B). At 2 dpci, *Imp-i* or H-overexpressing GSC clones and their appropriate control clones
287 occupied the niche in equal proportions (Fig. 7P; Table S2 #1 and #3; Fig. 7T; Table S4 #1, #3
288 and #5). By 14 dpci, *Imp-i* or H-overexpressing GSC clones occupied a majority of the GSC pool
289 compared to control clones (Fig. 7P; 44.38 ± 5.38% GSCs in *Imp-i* compared to 21.12 ± 1.98%
290 GSCs in control, $P \leq 0.0199$; see also Table S2 #4 vs #2; Fig. 7T; 63.92 ± 2.9% GSCs in H^{EP}
291 and 73.6 ± 6.05% in H^{GS} compared to 41.86 ± 3.67% GSCs in control, $P \leq 0.0001$; see also
292 Table S4, #6 vs #2 and #4 vs #2).
293 We previously showed that *chinmo*-mutant GSCs cause a significant drop in the average
294 total number of GSCs by evicting of their non-mutant GSC neighbors [33]. Here, we find that *Imp-i*

295 or H-over-expressing GSC clones similarly affect the GSC pool by causing a net loss in the
296 average total number of GSCs at 14 dpci (**Fig. 7Q**; 5.06 ± 0.37 GSCs in *Imp-i*, compared to 6.50
297 ± 0.43 GSCs in control, $P \leq 0.02$; see also **Table S2 #8** vs **#6**; **Fig. 7U**; 3.85 ± 0.19 GSCs in H^{EP}
298 and 4.08 ± 0.22 GSCs in H^{GS} compared to 5.17 ± 0.19 GSCs in control, $P \leq 0.0001$; see also
299 **Table S4 #12** vs **#8** and **#10** vs **#8**). Additionally, by 14 dpci non-mutant neighbor GSCs were
300 precipitously lost from the niche in the presence of *Imp-i* or H-overexpressing GSC clones but
301 not control GSC clones (**Fig. 7R**; 2.91 ± 0.33 non-mutant neighbor GSCs in *Imp-i* compared to
302 5.13 ± 0.37 in control, $P \leq 0.0001$; see also **Table S2 #12** vs **#10**; **Fig. 7V**; 1.67 ± 0.16 non-
303 mutant neighbor GSCs in H^{EP} and 1.22 ± 0.29 in H^{GS} compared to 3.18 ± 0.25 in control, $P \leq$
304 0.0001; see also **Table S4 #18** vs **#14, #16** vs **#14**). There was no statistical difference between
305 the number of control, *Imp-i*, or H-overexpressing GSC clones at 14 dpci (**Fig. 7S**; 1.38 ± 0.17
306 versus 1.92 ± 0.30, control and *Imp-i* clones, respectively, $P \leq 0.1191$; see also **Table S2 #16** vs
307 **#14**; **Fig. 7W**; 2.42 ± 0.12 GSCs in H^{EP} and 2.76± 0.24 in H^{GS} compared to 2.04 ± 0.17 GSCs in
308 control, $P \leq 0.25$ and $P \leq 0.54$, respectively; see also **Table S4 #24** vs **#20** and **#22** vs **#20**).
309 These data indicate that control, *Imp-i* or H-overexpressing GSC clones expand to a similar
310 extent, consistent our prior work on *chinmo*-mutant GSC clones. They also highlight that the
311 competitiveness of *Imp-i* or H-overexpressing GSC clones derives from their non-autonomous
312 effects on non-mutant neighbors. Additionally, we obtained similar results on all of these
313 parameters using an additional, validated *Imp-i* transgene (**Fig. S7F-I**; **Tables S1, #11-14** and
314 **S3**) [28]. Taken together, these results indicate that competitive GSCs exert their competitive
315 advantage by expelling neighbor GSCs..
316
317 **Discussion**
318 **Aging regulates the BMP/H/Imp/Chinmo axis in GSC testis niche**
319 Our study reveals how age-dependent changes in niche cells of the *Drosophila* testis
320 drive aging of the niche microenvironment. We demonstrate that declining BMP levels in niche
321 cells lead to the upregulation of the co-repressor H in GSCs. In turn, H represses expression of
322 the RBP Imp, thereby reducing levels of the key aging and competition factor Chinmo. Age-
323 dependent phenotypes are caused by reduced BMP in niche cells, increased H in GSCs or
324 reduced Imp/Chinmo in GSC, ultimately causing a decline in the GSC pool. Moreover, clonal
325 analyses indicate that GSCs lacking Imp or harboring robust H gain a competitive advantage in

326 niche residency over WT GSC neighbors. Altogether, our data link the age-related decline in
327 self-renewal cues to a cell-intrinsic H/Imp/Chinmo mechanism that drives GSC aging and
328 competition.

329 Our results suggest that Chinmo levels in GSCs regulate competition among WT GSCs
330 during aging, ultimately contributing to the significant decline in GSC numbers in aged testes.
331 Although Chinmo levels decrease overall with age, there is substantial variability in Chinmo
332 expression between individual GSCs (**Fig. 1D**). In a youthful environment, high Chinmo levels
333 repress expression of Pcan and Dg. However, as GSCs age and Chinmo levels decline, Pcan and
334 Dg become upregulated. Secreted Pcan accumulates around the niche, forming a progressively
335 expanding "moat" that alters the niche architecture. Within this altered environment, GSCs with
336 the lowest Chinmo—and consequently the highest Dg—are best equipped to remain in the niche.
337 In contrast, GSCs with relatively higher Chinmo and lower Dg are displaced and differentiate.
338 Thus, our findings suggest that among WT GSCs, those with the lowest Chinmo levels "win" the
339 competition for niche occupancy during aging.

340

341 **BMP production declines during aging**

342 Although the JAK-STAT ligand Upd also declines with age in the testis niche, Chinmo is
343 not regulated by STAT signaling in GSCs (**Fig. S1J-M**) [30,31]. Instead, we show that Chinmo is
344 positively regulated by the level BMPs in niche cells. Our data now provide direct evidence that
345 BMP production in testicular niche cells wanes over time, and this local reduction is sufficient to
346 cause age-dependent phenotypes in the niche microenvironment and in GSCs via Chinmo. Thus,
347 BMPs appear to be the principal extrinsic cues orchestrating testis aging. Interestingly, a similar
348 role for niche-derived BMPs has been shown for aging of the *Drosophila* ovary [56]. BMP
349 signaling is highly conserved, and studies in vertebrate models have demonstrated that
350 significant alterations in BMP signaling regulate aging of several tissues [57-59].

351 We find that overexpression of either Gbb or Dpp in testicular niche cells throughout
352 adulthood suppresses age-related changes in H, Chinmo, Pcan, Dg, and in GSC homeostasis.
353 Thus, both ligands can mitigate niche deterioration when artificially elevated (**Fig. 5K–N**). Prior
354 studies indicate that Gbb is more dominant under normal conditions, as *gbb* loss-of-function
355 mutants display severe GSC loss, whereas *dpp* hypomorphic mutants are less affected [39]. Further
356 work is needed to determine whether Gbb and Dpp act as homodimers or heterodimers to

357 regulate H, Imp, and Chinmo in aging GSCs.

358

359 **H is a Notch-independent regulator of aging**

360 We found that H exerts a Notch-independent effect on adult GSCs by repressing *Imp*
361 transcription. Although H is best known for antagonizing the Notch pathway, we did not detect
362 changes in the expression of Notch transcriptional reporters when manipulating H in GSCs (**Fig.**
363 **S6H-K**). Prior work has shown additional roles for H beyond direct Notch inhibition, including
364 modulation of EGFR signaling to promote vein development and regulation of apoptosis or cell
365 growth through diverse pathways [47,60]. Our findings place H downstream of BMP signaling, as
366 age-associated increases in H reduce Chinmo levels via repression of Imp. This indicates a
367 broader function for H in stem cell competency and aging that extends beyond Notch. Several
368 questions remain. For instance, it is not yet clear whether a specific threshold of H is needed to
369 repress *Imp* or precisely how BMPs regulate H. Mothers against decapentaplegic (Mad) is the
370 best-known transcriptional effector of BMP signaling in *Drosophila*: it becomes phosphorylated
371 by BMP receptors upon BMP ligand binding on the GSC and subsequently represses *bam*, a key
372 differentiation gene in female GSCs [61]. Investigating potential binding sites for the Mad within
373 the regulatory elements of *H* may clarify how external signals converge on the *H* locus to control
374 GSC aging and competitive dominance. It is tempting to speculate that transcriptional changes in
375 observed aged tissues might be caused by age-related increases in co-repressors [2].

376 **Parallels with mammalian Imp orthologs**

377 Our findings parallel those from a recent study on the mammalian ortholog of Imp,
378 IGF2BP1/2/3, in HSC aging [62]. In mice, IGF2BP2 is highly expressed in young HSCs but
379 becomes significantly downregulated with age, contributing to reduced stem cell function,
380 decreased metabolism-related gene expression, and age-related phenotypes. These parallels in
381 Imp/IGF2BP function across evolutionarily distant systems underscore the conserved role of this
382 family of proteins in stem cell maintenance and the aging process. However, whereas the
383 mammalian study highlights a predominantly intrinsic role of IGF2BP2 in HSC aging, our work
384 shows how niche-dependent factors regulate Imp in *Drosophila* GSCs. This suggests that
385 environmental cues influence Imp/IGF2BP activity in stem cells. Given the well-documented
386 effects of aging on niches in both invertebrates and vertebrates, it is plausible that extrinsic
387 regulatory pathways also control IGF2BP2 levels or function in mammalian HSCs. Unraveling

388 these mechanisms could clarify how systemic cues contribute to stem cell aging in higher
389 organisms.
390
391 **Limitations of the study**
392 While our data suggest that Dpp and Gbb produced by niche cells are sufficient to
393 modulate H expression in GSCs, we cannot exclude the possibility that additional cues from
394 other nearby cells, such as CySCs that also secrete Dpp or Gbb [36] and contribute to regulating H
395 in GSCs. Further tissue-specific knockdown or over-expression studies would be necessary to
396 clarify this point. In addition, we cannot conclude whether Dpp and Gbb form homodimers or
397 heterodimers when activating BMP signaling in GSCs. Determining the precise ligand
398 composition *in vivo* would require endogenously tagged alleles in mutant backgrounds designed
399 to distinguish between BMP ligand dimeric forms. Another limitation is the temporal resolution
400 of our experiments. While we examined changes at certain age intervals, the dynamic
401 progression of niche remodeling and GSC competition between these time points is not fully
402 captured. A more continuous sampling of various time points during adulthood using long-term
403 *ex vivo* live images would provide a clearer view of the intermediate steps in these processes.
404
405 **RESOURCE AVAILABILITY**
406 **Lead contact**
407 Further information and requests for resources and reagents should be directed to and will be
408 fulfilled by the Lead Contact, Chen Yuan Tseng (chenyuan1102@dragon.nchu.edu.tw).
409
410 **Materials availability**
411 Materials used in this study are available upon request to the lead contact, Chen-Yuan Tseng
412 (chenyuan1102@dragon.nchu.edu.tw)
413
414 **Data and code availability**
415 - Any additional information required to reanalyze the data reported in this paper is
416 available from the lead contact upon request.
417 - All data reported in this paper will be shared by the lead contact upon request.
418

419 **Acknowledgments**

420

421 We thank all members of the Bach and Tseng laboratories for their insightful discussions and
422 technical support. We are grateful to Dr. Jeremy J.-W. Chen (College of Medicine, National
423 Chung Hsing University) for assistance with the confocal microscope (LSM980), and we thank
424 the Instrument Center at National Chung Hsing University for help with the LSM900 confocal
425 microscope. We thank P. Rangan, N. Sokol, T. Volk, S. Baumgartner, L. Weaver, C. Desplan, T.
426 Lee, S. Bray, Bloomington *Drosophila* Stock Center (BDSC), Vienna *Drosophila* Resource
427 Center (VDRC) and Kyoto *Drosophila* Stock Center for antibodies and fly stocks. The BDSC is
428 supported by a grant from the Office of the Director of the NIH (P40OD018537). We are
429 grateful to FlyBase, supported by a grant from the National Human Genome Research Institute at
430 NIH (U41 HG000739). Work in the Bach lab is supported by grants from the NIH
431 (R01GM085075, R35GM156624-01, R03HD090422). Work in the Tseng lab is supported by
432 the Ministry of Science and Technology of Taiwan (MOST 111-2311-B-005-011-MY3), Taiwan
433 and National Chung Hsing University and Chun Shan Medical University (NCHU-CSMU
434 11204) and start-up funds from the Institute of Life Science, NCHU.

435

436 **Author contributions**

437 Conceptualization, C.Y.T. and E.A.B.; Investigation, Y.Z, Y.C.L., Y.T.W., P.K.C., S.L.C.,
438 L.S.H., H.J.H. and C.Y.T;. Manuscript writing. C.Y.T. and E.A.B.; Funding, C.Y.T. and E.A.B.;
439 Supervision, C.Y.T. and E.A.B.

440

441 **DECLARATION OF INTERESTS**

442 The authors declare no competing interests.

443

444 STAR★Methods

445 Key Resource Table

Reagent or Resource	SOURCE	IDENTIFIER
Antibodies		
Rat polyclonal anti-Chinmo (1:200)	Lesley Weaver (Indiana University Bloomington, USA)	
Guinea pig polyclonal anti-Vasa (1:200)	Bach lab	
Rat polyclonal anti-Imp (1:200)	Claude Desplan (New York University, USA)	
Rabbit polyclonal anti-GFP (1:1000)	Invitrogen	Cat# A-11122, RRID: AB_221569
Rabbit polyclonal anti-Pcan (1:1000)	Stefan Baumgartner (Lund University, Sweden)	
Chicken polyclonal anti-Vasa (1:200)	Prashanth Rangan (Icahn School of Medicine at Mount Sinai, USA)	
Chicken polyclonal anti-GFP (1:1000)	Abcam	Cat# ab13970, RPID: AB_300798
Guinea pig anti-Laminin (1:1000)	T. Volk (Weizmann Institute, Israel)	
Rabbit polyclonal anti-Dg (1:500)	Stefan Baumgartner	
Mouse monoclonal anti-Fasciclin III (Fas3) (1:100)	Developmental Hybridoma Bank (DSHB)	Cat# 7G10, RRID: AB_528238
Mouse anti-Glass bottom boat (Gbb) (1:200)	DSHB	Cat# 3D6-24, RRID: AB_2618111
Mouse monoclonal anti-GFP (GFP) 1:500	ABclonal	Cat# AE012, RRID: AB_2770402

Cy3-AffiniPure Donkey Anti-Mouse IgG (1:400)	Jackson ImmunoResearch Labs	Cat# 715-165-150, RRID: AB_2340813
Alexa Fluor 488-AffiniPure Donkey Anti-Rabbit IgG (H+L) (1:400)	Jackson ImmunoResearch Labs	Cat# 711-545-152, RRID: AB_2313584
Anti-Dig-POD	Roche	Cat# 11207733910, RRID: AB_514500
Cy3-AffiniPure Donkey Anti-Rabbit IgG (H+L) (1:400)	Jackson ImmunoResearch Labs	Cat# 711-165-152, RRID: AB_2307443
Alexa Fluor 488-AffiniPure Donkey Anti-Rat IgG (H+L) (1:400)	Jackson ImmunoResearch Labs	Cat# 712-545-150, RRID: AB_2340683
Cy3-AffiniPure Donkey Anti-Rat IgG (H+L) (1:400)	Jackson ImmunoResearch Labs	Cat# 712-165-150, RRID: AB_2340666
Cy5-AffiniPure Donkey Anti-Rat IgG (H+L) (1:400)	Jackson ImmunoResearch Labs	Cat# 712-175-150, RRID: AB_2340671
Cy3-AffiniPure Donkey Anti-Chicken IgY (IgG) (H+L) (1:400)	Jackson ImmunoResearch Labs	Cat# 703-165-155, RRID: AB_2340363
Cy5-AffiniPure Donkey Anti-Chicken IgY (IgG) (H+L) (1:400)	Jackson ImmunoResearch Labs	Cat# 703-175-155, RRID: AB_2340365
Cy3-AffiniPure Donkey Anti-Guinea Pig IgG (1:400)	Jackson ImmunoResearch Labs	Cat# 706-165-148, RRID: AB_2340460
Cy5-AffiniPure Donkey Anti-Guinea Pig IgG (H+L) (1:400)	Jackson ImmunoResearch Labs	Cat# 706-175-148, RRID: AB_2340462
Chemicals, Peptides, and Recombinant Proteins		

VECTASHIELD Mounting Medium with DAPI	Vector Laboratories	Cat# H-1200, RRID: AB_2336790
ibidi Mounting Medium With DAPI	ibidi	Cat# 50011
Paraformaldehyde, 16% w/v aq. soln., methanol free	Thermo Fisher Scientific	Cat# 43368-9L
Digoxigenin-11-UTP	Roche	Cat# 3359247910
Blocking Reagent for RNA-FISH	Roche	Cat# 11096176001
TSA Plus Fluorescence Kits; PerkinElmer	Akoya Biosciences	Cat# NEL745001KT
Experimental Models: Organisms/Strains		
D. melanogaster; w^{1118}	Bach lab	
D. melanogaster; *y w*	Bach lab	
D. melanogaster; *Oregon-R*	Hwei-Jan Hsu lab (Academia Sinica, ICOB)	
D. melanogaster; *UASp-3HA-Stat92E*$^{FL\#5}$	Bach lab	
D. melanogaster; P[GawB]tj^{NP1624} *(tj-Gal4)*	Bach lab	FlyBase: FBal0326545
D. melanogaster; *Stat92E*^{F}, *e*	Bach lab	FlyBase: FBst0024757
D. melanogaster; *Stat92E*^{85c9}, *e*	Bach lab	
D. melanogaster; *y, w, hs-flp*^{122}*/Y; ubi-GFP, FRT*^{40A}	Bach lab	
D. melanogaster; *w; P[ry[+t7.2]=neoFRT]*^{40A}	Bloomington *Drosophila* Stock Center (BDSC)	BDSC: 5074 FlyBase: FBst005074

D. melanogaster; *y, w, hs-flp*^{122}, *tub-Gal4, UAS-nls-GFP; tub-Gal80, FRT*^{40A}*/ CyO*	Bach lab	
D. melanogaster; *y, w, hs-flp*^{122}, *tub-Gal4, UAS-nls-GFP; FRT*^{82B} *tub-Gal80/ TM3*	Bach lab	
D. melanogaster; y^{d2} *w*^{1118} *P[ey-FLP.N]2;FRT*^{82B} *Dcr-1*^{Q1147X}*/ TM3* (*Dcr-1*$^{-/-}$)	BDSC	BDSC: 32066 FlyBase: FBst0032066
D. melanogaster; y, w, hs-flp^{122}*; FRT*^{42D} *ubi-GFP/ CyO*	Bach lab	
D. melanogaster; y^{d2} *w*^{1118} *P[ey-FLP.N]2 P[5xglBS-lacZ.38-1]TPN1; P[neoFRT]*^{42D} *P[lacW]AGO1*^{k08121}*/ CyO y*$^{+}$ (*AGO1*$^{-/-}$)	Kyoto stock center	Kyoto:111238 FlyBase: FBst0314058
D. melanogaster; y^{1} *sc* v*^{1} *sev*^{21}*; P[TRiP.HMS00064]attP2/TM3, Sb* (*drosha-i*)	BDSC	BDSC: 33657 FlyBase: FBst0033657
D. melanogaster; *w*; P[y[+t7.7] w[+mC]=UAS-mCherry.mir-let7.sponge.V2] attP40; P[y[+t7.7] w[+mC]= UAS-mCherry.mirlet7. sponge.V2]attP2/ TM6B, Tb* (*mir-let7.sponge*)	BDSC	BDSC: 61365 FlyBase: FBst0061365
D. melanogaster; *y, w; P[w+, nos-GAL4 VP16]* on II (*nos-Gal4*)	Bach lab	
D. melanogaster; *w*^{1118}*; P[w[+mC]=UAS-lacZ.NZ]J312* (*UAS-lacZ*)	BDSC	BDSC: 3956 FlyBase: FBst003956

D. melanogaster; y, w, hs-flp^{122}*; nos-FRT-STOP-SV40-polyA-STOP-FRT-Gal4, UASp-gfp/CyO* (*nos* flip-out cassette)	Hsu lab	
D. melanogaster; y^1 w^* *Mi[PT-GFSTF.2]Imp*$^{MI05901\text{-}GFSTF.2}$ (Imp::GFP$^{\#1}$)	BDSC	BDSC: 60237 FlyBase: FBst0060237
D. melanogaster; UAS-Imp-RM-3Xflag attP40/ CyO (*UAS-Imp*)	Tzumin Lee (Janelia Research Camp, USA)	
D. melanogaster; w^*, *P[PTT-un]Imp*^{ZCL2884X} (Imp::GFP$^{\#2}$)	Kyoto *Drosophila* Stock Center (Kyoto)	Kyoto: 110921 FlyBase: FBst0307963
D. melanogaster; y^1 v^1; *P[TRiP.HMS00036]attP2/TM3, Sb* (*chinmo-i*)	BDSC	BDSC: 33638 FlyBase: FBst0033638
D. melanogaster; y^1 v^1; *P[TRiP.GL00660]attP40* (*Imp-i* B#38219)	BDSC	BDSC: 38219 FlyBase: FBst0038219
D. melanogaster; w^{1118}; *P[GD9232]v20321* (*Imp-i* V#20321)	Vienna *Drosophila* Resource Center (VDRC)	VDRC: 20321 FlyBase: FBst0453703
D. melanogaster; *w; UAS-5'UTR-chinmo-3'UTR* (*UAS-chinmo*)	Bach lab	
D. melanogaster; y^1 sc^* v^1 sev^{21};*P[TRiP.HMS00141]attP2* (*UAS-Dcr-1-i*)	BDSC	BDSC: 34826 FlyBase: FBst0034826
D. melanogaster; y^1 v^1; *P[y[+t7.7]=CaryP]attP2* (*UAS-control-i*)	BDSC	BDSC: 36303 FlyBase: FBst0036303

D. melanogaster; w^{1118}; P[GD9477]v33011 (*syp-i*)	VDRC	VDRC: 33011 FlyBase: FBst0459885
D. melanogaster; y^1 sc^* v^1 sev^{21};P[TRiP.HMS01989]attP2 (*Ets21C-i*)	BDSC	BDSC: 39069 FlyBase: FBst0039069
D. melanogaster; y^1 sc^* v^1 sev^{21};P[TRiP.HMS01182]attP2 (*H-i*)	BDSC	BDSC: 34703 FlyBase: FBst0034703
D. melanogaster; y^1 sc^* v^1 sev^{21}; P[TRiP.JF02624]attP2 (*H-i #2*)	BDSC	BDSC: 27315 FlyBase: FBst0027315
D. melanogaster; y^1 v^1; P[TRiP.HMS02286]attP2 (*p53-i*)	BDSC	BDSC: 41720 FlyBase: FBst0041720
D. melanogaster; *w*, TI[CRIMIC.TG4.1]HCR60128-TG4.1/TM3, Sb* (*H-Gal4*)	BDSC	BDSC: 93469 FlyBase: FBst0093469
D. melanogaster; *w*, UASp-myristoylated-GFP* (*UAS-myrGFP*)	Hsu lab	
D. melanogaster; *w*, UASp-mCD8-GFP* (*UAS-mCD8-GFP*)	Hsu lab	
D. melanogaster; *w*, Dpp::mCherry*	Hsu lab	
D. melanogaster; *w*, Hairless::GFP* (H::GFP) on II	Sarah Bray (University of Cambridge, England)	
D. melanogaster; *w*; Suppressor of Hairless-GFP* (Su(H)::GFP) on III	Bray lab	
D. melanogaster; *w*; Notch responsive element-GFP*	Bray lab	

(*NRE-GFP*)		
D. melanogaster; *w*; Notch responsive element-RFP* (*NRE-RFP*)	Bray lab	
D. melanogaster; y^1 *w*, UAS-lacZ/CyO; UAS-lacZ/ TM6C*	Bach lab	
D. melanogaster; *w* upd-Gal4, tub-Gal80*^{ts} (*upd-Gal4*^{ts})	Bach lab	
D. melanogaster; *w*;; P[w[+mC]=UAS-dpp.GFP.T]3/TM3, Sb* (*UAS-Dpp::GFP*)	BDSC	BDSC: 53716 FlyBase: FBst0053716
D. melanogaster; y^1 *w*; P[w[+mC]=UASp-gbb.GFP]3.3/ CyO* (*UAS-Gbb::GFP*)	BDSC	BDSC: 63057 FlyBase: FBst0063057
D. melanogaster; y^1 *w*; P[w[+mC]=UASp-gbb.GFP]3.3/ CyO* (*UAS-Gbb-GFP*)	BDSC	BDSC: 63057 FlyBase: FBst0063057
D. melanogaster; y^1 *w* ; P[EPgy2]H*^{EY03696} (H^{EY}) = UAS-H	BDSC	BDSC: 15672 FlyBase: FBst0015672
D. melanogaster; w^*; *P[w[+mGS]=GSV1]H*$^{EP-211}$ (H^{EP}) = UAS-H	BDSC	BDSC: 43408 FlyBase: FBst0043408
D. melanogaster; *y,* w^{67c23}; *P[GSV6,GS11776]* (H^{GS}) = UAS-H	Kyoto	Kyoto: 205338 FlyBase: FBti0104065
Oligonucleotide		
HCR probe of *chinmo-RA, -RD, -RG, RH*	Molecular Instruments, Inc.	LOT: PRJ996

HCR probe of *chinmo-RE, -RF*	Molecular Instruments, Inc.	LOT: PRJ998
HCR probe of *chinmo-RH*	Molecular Instruments, Inc.	LOT: PRJ997
Software and Algorithms		
ImageJ/Fiji	Fiji	http://fiji.sc/
Photoshop/Illustrator	Adobe	https://www.adobe.com/products/
Excel	Microsoft	https://products.office.com/en-us/excel
Prism 9	GraphPad	https://www.graphpad.com/
ZEN blue	Zeiss	https://www.zeiss.com/microscopy/en/products/software/zeiss-zen.html

446

447 Experimental model and subject details

448 *Drosophila melanogaster* strains used in this study are listed in the Key Resources Table. Flies
449 were raised at 25°C on standard fly food except *nos* flip-out cassette crosses, which were
450 maintained at 18°C until eclosion, and the adult flies were transferred to 29°C. We used only
451 adult *Drosophila* males in this study and the vials were changed daily. The *Drosophila* stocks
452 used in this study as follows: *nos-Gal4-VP16* [63]; *UASp-3HA-Stat92E*$^{FL\#5}$ [64]; *Stat92E*^{F} [65];
453 *Stat92E*^{85c9} [66]; *tj-Gal4* [67]; *UAS-LacZ* (BDSC #3956); *UAS-drosha-i* (BDSC#33657); *UAS-*
454 *chinmo-i* (BDSC #33638); *UAS-Imp-i* (BDSC #38219); *UAS-Imp-i* (VDRC #20321); *UAS-Dcr1-*
455 *i* (BDSC #34826); *UAS-control*-i (BDSC #36303); *UAS-syp-i* (VDRC #33011); *UAS-Ets21C-i*
456 (BDSC #39069); *UAS-H-i* (BDSC #34703); *UAS-H-i* (BDSC#27315); *UAS-p53-i* (BDSC
457 #41720); *H-Gal4* (BDSC#93469); *UAS-H*^{EY} (BDSC#15672); *UAS-H*^{EP} (BDSC#43408); *UAS-H*^{GS}
458 (Kyoto#205338); *Imp-GFP*$^{\#1}$ (BDSC#60237) and *Imp-GFP*$^{\#2}$ (Kyoto#110921); *UAS-Dpp::GFP*
459 (BDSC#53716); *UAS-Gbb::GFP* (BDSC#63057); *UAS-Imp* (Tzumin Lee lab, University of
460 Michigan, USA); *UAS-5'UTR-chinmo-3'UTR* [68]; *UASp-NICD and Dpp::mCherry* (Hwei-Jan
461 Hsu lab, Academia Sinica, Taiwan); *NRE-GFP*, *NRE-RFP, Hairless::GFP* and *Su(H)::GFP*
462 (Sarah Bray lab, University of Cambridge, UK); *tub-Gal80*^{ts}. For a list of full genotypes by
463 figures, see Table S5.

464

465 Detailed methods

466 RNAi-mediated gene depletion

467 To identify genes that genetically interact with Imp, we employed an RNA interference (RNAi)
468 approach in *Drosophila*. Male UAS-RNAi transgenic flies (targeting *H*, *Ets21C*, or *p53*) were
469 crossed with virgin females carrying the *nos*-Gal4 driver in combination with the temperature-
470 sensitive *tub-Gal80*^{ts}. All crosses were initially maintained at 18°C to minimize leaky expression
471 of the RNAi constructs during development. 2- to 3-day-old adult males of the correct genotype
472 were transferred to fresh vials and shifted to 29°C to induce robust RNAi expression. For the
473 initial screening in Fig. S5A, cohorts of male flies were reared at 29 °C for 14 days prior to
474 dissection, allowing assessment of Imp protein levels. A separate set of males were maintained at
475 29°C for 2, 28 or 42 days to investigate later-onset phenotypes or age-dependent effects.
476
477 Generation of STAT-deficient GSCs
478 *Stat92E*^{F} is a temperature-sensitive allele, and viable adults carrying *Stat92E*^{F} can be obtained if
479 this allele is *in trans* to a hypomorphic allele like *Stat92E*^{85c9} and if the cross is reared at the
480 permissive temperature 16°C until eclosion [65]. When *Stat92E*^{F}/*Stat92E*^{85c9} adults are shifted to
481 the restrictive temperature 29°C, Stat92E function is lost. *Stat92E*-mutant GSCs lose adhesion to
482 the niche and differentiate. However, *Stat92E*-mutant GSCs can be maintained by somatic
483 support cells (i.e., *tj-Gal4*-positive cells) expressing a full-length Stat92E transgene (i.e., *UASp-*
484 *3HA-Stat92E*$^{FL\#5}$)[36]. We generated *y, w/Y; tj-Gal4/UASp-3HA-Stat92E*$^{FL\#5}$*; Stat92E*^{F}*/Stat92E*^{85c9}
485 males or *w/Y; Stat92E*^{F} *e/+* controls, upshifted them to 29°C for 7 days, and then dissected testes
486 and stained them for Chinmo.
487
488 GSC clonal induction
489 Negatively-marked GSC clones were generated using the FLP/FRT technique after a single 1-
490 hour heat shock at 37°C in 2-day-old adult males [69]. Males were returned to 25°C until dissection
491 at 2, 7, or 14 dpci. Positively marked clones were generated in 2-day old adult males by the
492 MARCM technique after a single 1-hour heat shock in Figs. 7 and S1 and *nos* flip-out technique
493 in Figs. 7 and S7, after 30-minute heat shock at 37°C [54,55]. Males were returned to 25°C until
494 dissection at 2 or 14 dpci. Lineage-wide mis-expression or depletion was achieved using the
495 Gal4/UAS system [70]. A *Gal80*^{ts} transgene was for thermo-sensitive control of Gal4 [71].
496
497 Immunofluorescence

498 Dissections and immunostaining were carried out as previously described [33]. Briefly, testes were
499 dissected in 1x phosphate buffered saline (PBS), fixed for 30 minutes in 4% paraformaldehyde
500 (PFA) in 1xPBS, washed twice for 0.5 hours at 25°C in 1xPBS with 0.5% Triton X-100, and
501 blocked in PBTB (1xPBS 0.2% Triton X-100 and 1% bovine serum albumin) for 1 hour at 25°C.
502 Primary antibodies were incubated overnight at 4°C. Samples were washed twice for 30 minutes
503 in PBTB and incubated for 2 hours in secondary antibody in PBTB at 25°C and then washed
504 twice for 30 minutes in 1xPBS with 0.2% Triton X-100. Samples were mounted in Vectashield
505 with DAPI (Vector Laboratories) or ibidi mounting Medium with DAPI (ibidi). Confocal images
506 were captured using Zeiss LSM710, LSM900 and LSM980 microscopes with a 63x objective
507 and 10–20 z-stacks (interval 1 µm) using lasers at 405, 488, 561, and 640 nM.
508
509 RNA isolation and quantitative real-time reverse transcription PCR (qRT-PCR)
510 To measure gene expression in the anterior region of *Drosophila* testes (from GSCs to the
511 spermatogonial stage), 150–200 testes were carefully dissected from adult males using fine steel
512 pins under a stereomicroscope. The dissected tissue was immediately collected into lysis buffer,
513 and total RNA was extracted using the Arcturus PicoPure™ RNA Isolation Kit (Thermo Fisher
514 Scientific), following the manufacturer's instructions. Next, 0.5 µg of total RNA was reverse-
515 transcribed into complementary DNA (cDNA) using an M-MLV Reverse Transcription Kit
516 (Protech Technology Enterprise Co., Ltd) with oligo(dT) primers. The resultant cDNA was
517 diluted appropriately for downstream applications. Gene expression levels of *Imp* and *H* were
518 normalized against the housekeeping genes *rpl19* and *rpl32*. qPCR reactions were set up using
519 the KAPA SYBR® FAST qPCR Master Mix (Kapa Biosystems) on an ABI Prism™ real-time
520 PCR system (Applied Biosystems). Each sample was run in triplicate to ensure technical
521 reproducibility, and three biological replicates were analyzed per condition. All primer
522 sequences used in this study are listed in Table S6.
523
524 Hybridization Chain Reaction - Fluorescent *in Situ* Hybridization (HCR-FISH) and RNA-FISH
525 The HCR RNA probes against different *chinmo* mRNA isoforms, the HCR amplifier, and
526 reagents for the hybridization, wash, amplification buffers were purchased from Molecular
527 Instruments, Inc., HCR-FISH was performed according as previously described [33]. RNA FISH
528 was adapted from [72]. Briefly, the immunostaining procedure testes were fixed in 4% PFA in

529 0.1% Triton X-100 in 1xPBS-DEPC for 30 minutes at 25°C, washed twice with 0.5% Triton X-
530 100 in 1xPBS-DEPC for 30 minutes at 25°C. Samples were blocked in 0.1% Triton X-100 in
531 1xPBS-DEPC with 50 µg/mL heparin and 250 µg/mL yeast tRNA (PBTH), and then they were
532 then incubated with primary antibodies overnight at 4°C. The next day, the samples were washed
533 twice in PBTH for 30 minutes. Samples were then incubated with fluorescently labeled
534 secondary antibodies in PBTH for 2 hours at 25°C. Samples were washed twice in PBTH for 30
535 minutes at 25°C. Samples were then dehydrated and rehydrated with a series of ethanol washes
536 (25%, 50%, 75%, 100%) in 1xPBS-DEPC for 10 minutes at 25°C. Samples were treated for 3
537 minutes with 50 µg/mL Proteinase K, which was then inactivated by washing with 0.2% glycine
538 twice in 1xPBS-DEPC for 5 minutes at 25°C. After Proteinase K treatment, the samples were
539 fixed again in 4% PFA in 1xPBS-DEPC for 30 minutes at 25°C. The samples were pre-
540 hybridized in freshly hybridization buffer+ (HyB^+) containing 50% formamide, 5xSSC, 50
541 µg/mL heparin and 250 µg/mL yeast tRNA, 10 µg/mL Salmon sperm DNA with 0.1% Tween
542 20) for 10 minutes at 25°C and then incubated antisense *Imp* RNA probe in HyB^+ overnight (12 -
543 16 hour) at 55°C. The sample was washed by Hyb+, rinsed in 2xSCC, and washed with PBT for
544 10 minutes. The samples were incubated with an anti-DIG antibody conjugated to horseradish
545 peroxidase (HRP, Roche, 11207733910) at 4°C overnight. Finally, probes were detected using a
546 TSA™ Cy3 kit (NEL704A001KT), following the manufacturer's instructions. The antisense Dig-
547 labeled *Imp* probe was made using open reading frame (ORF) PCR amplicons from
548 complementary DNA libraries.
549
550 Quantification and statistical analysis
551 Quantification of Chinmo, Imp, Imp::GFP and H::GFP in GSCs, Dpp::mCherry and Gbb in the
552 GSC niche
553 Confocal Z-stacks were captured at 1 µm intervals to encompass all niche cells (typically 16–20
554 slices per testis). Fluorescence intensities of Chinmo, Imp, Imp::GFP, and H::GFP were
555 measured using ImageJ in a single Z-slice taken at the maximal width of each GSC. In clonal
556 experiments, the intensities of Chinmo and Imp in the mutant or knockdown GSCs were
557 normalized to those of a non-mutant neighbor GSC within the same testis. Each data point
558 represents one GSC or testis. For Dpp::mCherry and Gbb, signals were also measured in the z-
559 slice containing the largest area of the niche. The background fluorescence was recorded from

560 the nucleus of a muscle cell and subtracted from each measurement. Each data point here
561 represents one testis.
562
563 Quantification of Dg expression at the GSC-niche interface
564 We captured confocal Z-stacks (at 1 μm intervals) encompassing all niche cells (typically 16-20
565 slices). We measured Dg fluorescence intensity by ImageJ in single z slices at the area of
566 maximal contact of a GSC with the niche. The background signal was measured in the nucleus of
567 a gonialblast then subtracted from each GSC-niche measurement. In the mis-expression/
568 knockdown experiments, each data point represents the intensity of Dg in one GSC. In clonal
569 analyses, the fluorescence intensity of Dg at the GSC-niche interface of the clone was
570 normalized to that of a non-mutant neighbor GSC in the same testis. In the clonal analyses, each
571 data point represents one testis.
572
573 Quantification of *chinmo* and *Imp* mRNAs in the testis
574 We captured confocal Z-stacks (at 1 μm intervals) encompassing all niche cells and GSCs. We
575 measured the number of fluorescence dots in the group of niche cells and in the single GSC. In
576 niche analyses, each point represents niche cells. In GSC analyses, each point represents a single
577 GSC.
578
579 Quantification of Pcan intensity in the testicular lumen
580 We captured confocal Z-stacks (at 1 μm intervals) encompassing all niche cells (typically 16-20
581 slices). We measured the maximum area of Pcan fluorescence intensity by ImageJ in single z
582 slices at the area near the niche. The background signal was measured in the nucleus of GSC
583 and then subtracted from each other in the same testis. Each data point represents a single testis.
584
585 Quantification of fold change in Pcan/Lan-positive Testes
586 Confocal Z-stacks (1 μm intervals) were captured to encompass all niche cells (typically 16–20
587 slices) in each testis, and the samples were stained with Pcan or Lan. A niche was counted as
588 "Pcan/Lan-positive" if the ECM protein was detectable adjacent to at least one niche cell in any
589 confocal slice. To quantify the fold change, we first calculated the percentage of Pcan/Lan-
590 positive testes in each experimental condition and then divided that percentage by the

591 corresponding percentage in the control. This ratio reflects the relative increase (or decrease) in
592 Pcan/Lan-positive niches compared to control.
593
594 Statistical analysis
595 Statistical analyses were performed using two-tailed Student's t-tests, except for Figs. 3E, 3M,
596 5M, 6S, 7K, 7O, S1D, S7E and Table S1, which were performed using χ^2 tests. Data were
597 analyzed by GraphPad Prism and Microsoft Excel. Statistical significance was assumed by $P \leq$
598 0.05. Individual P values are indicated. Data are represented by the mean and standard error of
599 mean (SEM).
600
601

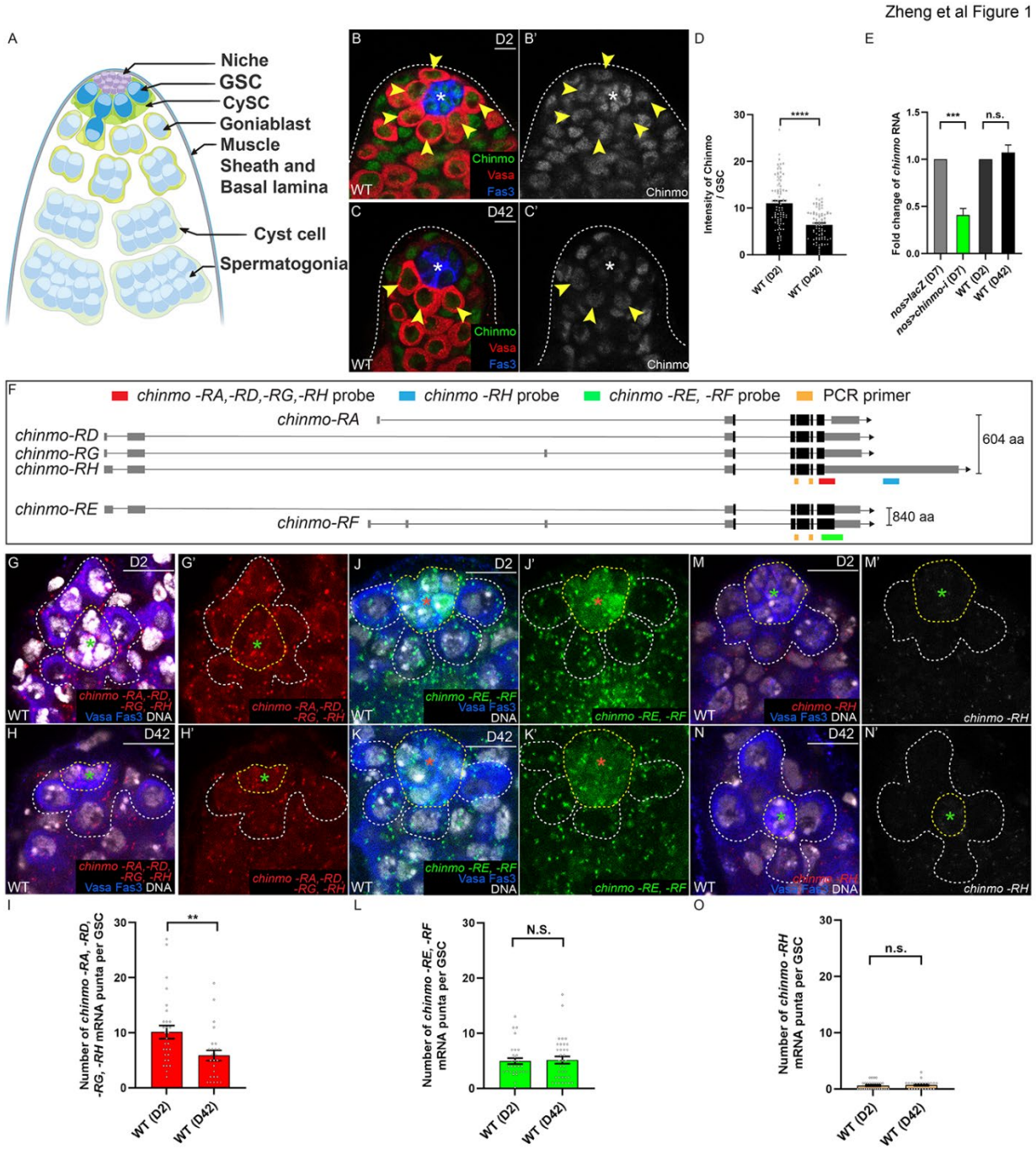

FIGURE LEGENDS

Figure 1. *chinmo* mRNA is post-transcriptionally regulated in GSCs during aging.

(A) The adult *Drosophila* testis. A GSC makes direct contact with the niche and divides to produce a gonialblast (Gb), which undergoes transit-amplifying divisions to produce a 16-cell spermatogonia that undergoes meiosis and differentiates into sperm. CySCs divide to produce cyst cells, two of which envelope a Gb and its descendants.

609 (B-D) Confocal images of WT testes in young (D2) (A) and aged (D42) (B) testes stained for.
610 Chinmo (green). Arrowheads indicate GSCs. (C) Graph showing the relative intensity of Chinmo
611 protein between D2 (A) and D42 (B) GSCs.
612 (E) Graph showing the relative change of *chinmo* mRNA in *nos>lacZ* (control, gray) versus
613 *nos>chinmo-i* (green) GSCs at D7 and the relative change of *chinmo* mRNA in D2 and D42
614 GSCs.
615 (F) Schematic of the six *chinmo* mRNA transcript (-*RA*, -*RD*, -*RE*, -*RF,* -*RG*, -*RH*). Exons (gray
616 boxes), introns (lines), and coding regions (black boxes) are shown. *chinmo*-*RA*, -*RD*, -*RG*, and -
617 *RH* encode a 604 aa protein, whereas *chinmo*-*RE* and -*RF* encode an 840 aa protein. The orange
618 boxes indicates the PCR primers spanning all *chinmo* transcripts. HCR probes for *chinmo*
619 isoforms are shown in red for -*RA,* -*RD,* -*RG,* -*RH*, in blue for -*RH*, and in green for -*RE,* -*RF*.
620 (G-O) Confocal images of HCR-FISH for *chinmo* mRNA in D2 (G, J, M) or D42 (H, K, N) in
621 WT testes. Dashed white and yellow lines indicate GSCs and niche cells, respectively.
622 Arrowheads indicate GSCs.
623 (G-I) Probe for *chinmo*-*RA,* -*RD,* -*RG*, and -*RH* transcripts (red) in F (D2) and G (D42),
624 quantified in I.
625 (J-L) Probe for *chinmo*-*RE* and -*RF* transcripts (green) in I (D2) and J (D42), quantified in L.
626 (M-O) Probes for *chinmo*-*RH* transcripts (red) in L (D2) and M (D42), quantified in O.
627 Asterisks in indicate the niche. DAPI labels DNA; Vasa labels germ cells; Fas3 labels niche
628 cells.
629 Scale bars = 10 μm.
630 In D, E, I, L, and O, error bars represent SEM. ** $P \leq 0.01$; *** $P \leq 0.001$; **** $P \leq 0.0001$;
631 n.s. indicates no significance, as determined by Student's t-test (see STAR Methods).
632

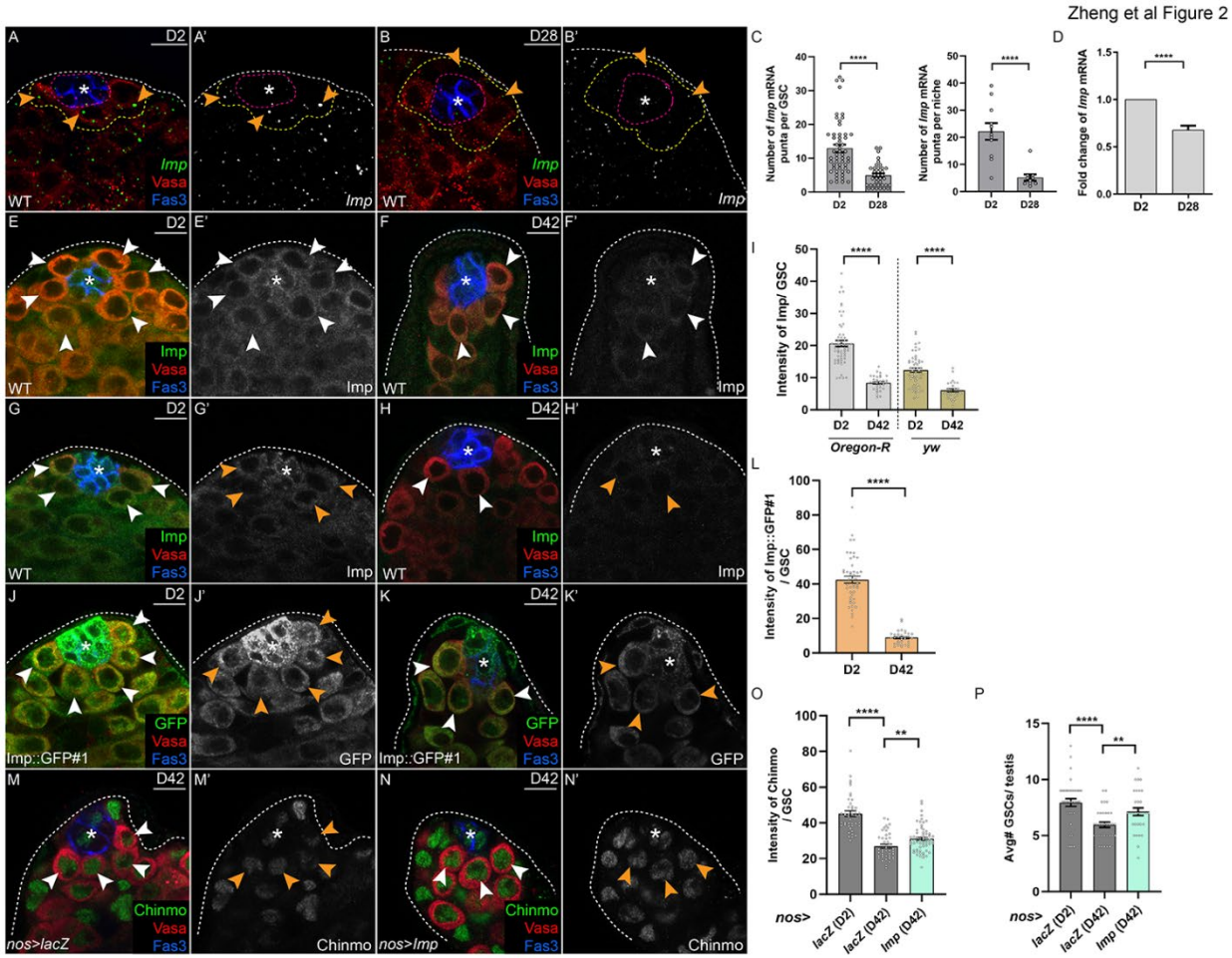

Figure 2. Imp positively regulates Chinmo protein expression in GSCs during aging.

(A-C) Confocal images of RNA-FISH for *Imp* mRNA (green) in young (D2) testes (A) and middle-aged (D28) testes (B). The yellow and blue dashed lines outline GSCs and niche cells, respectively. Graph in C shows the average number of *Imp* mRNA puncta per GSC (left) and per niche cell (right).

(D) qRT-PCR of *Imp* mRNA in D2 and D28 WT testes.

(E–I) Confocal images of Imp protein (green) in WT D2 (E, G) and D42 (F, H) testes, quantified in I.

(J-L) Confocal images of Imp::GFP protein trap #1 (green) in D2 (J) and D42 (K) testes, quantified in L.

(M-O) Confocal images of Chinmo (green) in D42 *nos>lacZ* (M) or D42 *nos>Imp* (N) testes, quantified in O.

(P) Graph showing the number of GSCs in D2 or D42 *nos>lacZ* (gray bars) or D42 *nos>Imp*

647 (light blue bars) testes.

648 In E, F, G, H, J, K, M, and N, arrowheads indicate GSCs, and asterisks indicate the niche. Vasa

649 labels germ cells; Fas3 labels niche cells.

650 Scale bars = 10 μm.

651 In C, D, I, L, O, and P, error bars represent SEM. ** $P \leq 0.01$; **** $P \leq 0.0001$; n.s. indicates

652 no significance, as assessed by Student's t-test.

653

654

655

656

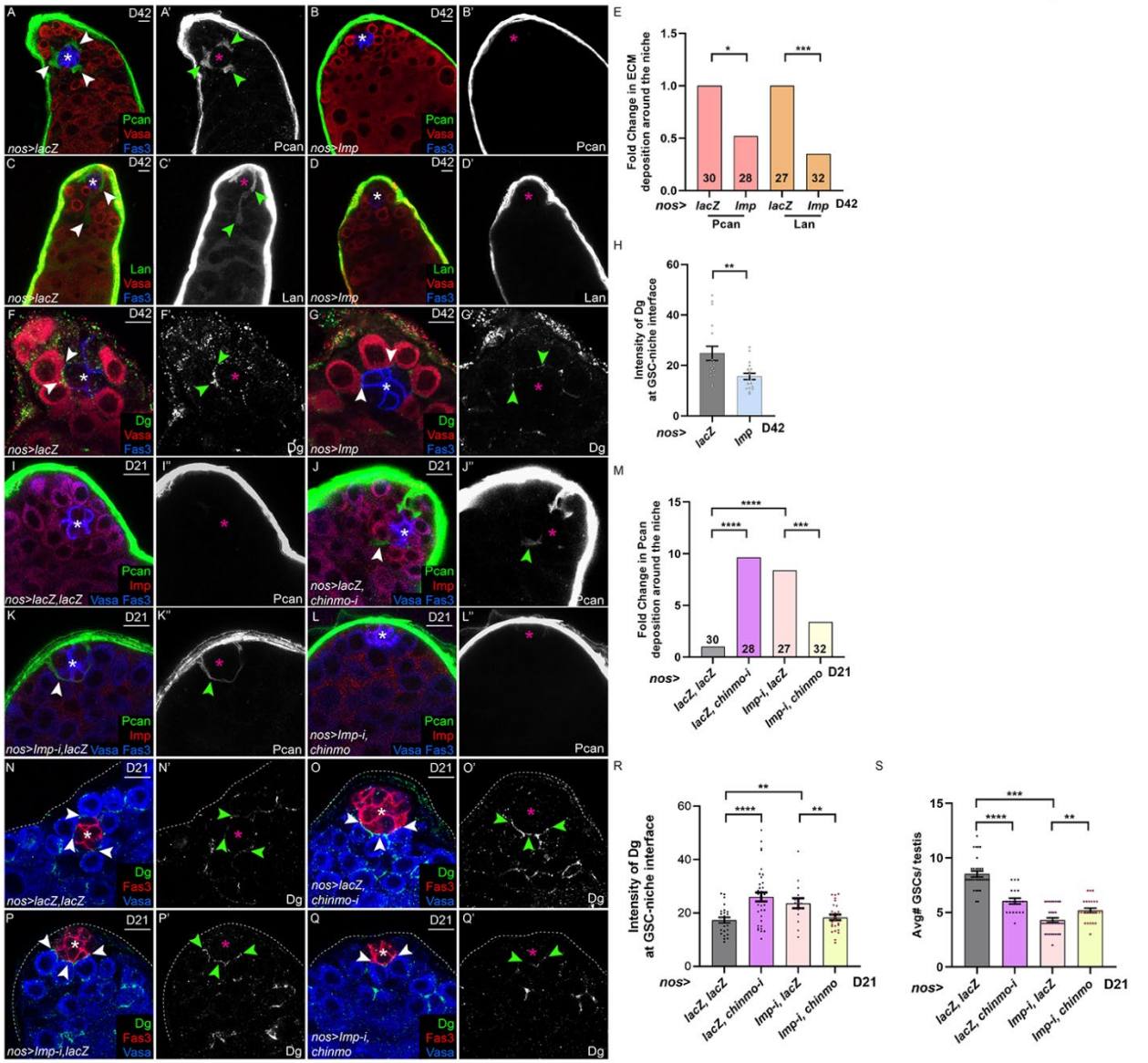

Figure 3. Imp controls aging of the testis stem cell niche via Chinmo.

(A–H) Confocal images showing Pcan (green in A, B), Lan (green in C, D), or Dg (green in F, G) proteins in D42 *nos>lacZ* (A, C, F) or D42 *nos>Imp* (B, D, G) testes, quantified in E (for Pcan and Lan) and H (for Dg). Arrowheads in A, C mark ectopic Pcan or Lan surrounding the niche. Sample numbers for each genotype were indicated in each bar. In F, G, arrowheads show increased Dg at the GSC–niche interface in *nos>lacZ* (F) compared to *nos>Imp* (G).

(I–L) Confocal images of Pcan (green) in D21 testes in *nos>lacZ, lacZ* (I), *nos>lacZ, chinmo-i* (J), *nos>Imp-i, lacZ* (K), and *nos>Imp-i, chinmo* (L). Arrowheads in (J, K) indicate ectopic Pcan around the niche.

667 (M) Graph showing the fold change in Pcan surrounding the niche in D21 testes of the genotypes
668 shown in (I–L).
669 (N–R) Confocal images of Dg (green) in D21 testes of the genotypes shown in (I–L), quantified
670 in R. Arrows indicate Dg the GSC–niche interface.
671 (S) Graph showing that the average number of GSCs in the genotypes shown in (I–L).
672 Asterisks in indicate the niche. Vasa labels germ cells; Fas3 labels niche cells.
673 Scale bars = 10 μm.
674 In H, R and S, error bars represent SEM. * $P \leq 0.05$; ** $P \leq 0.01$; *** $P \leq 0.001$; **** $P \leq$
675 0.0001 as assessed by Student's t-test in H, R, S, and by χ^2 test in E and M.
676
677
678
679

Zheng et al Figure 4

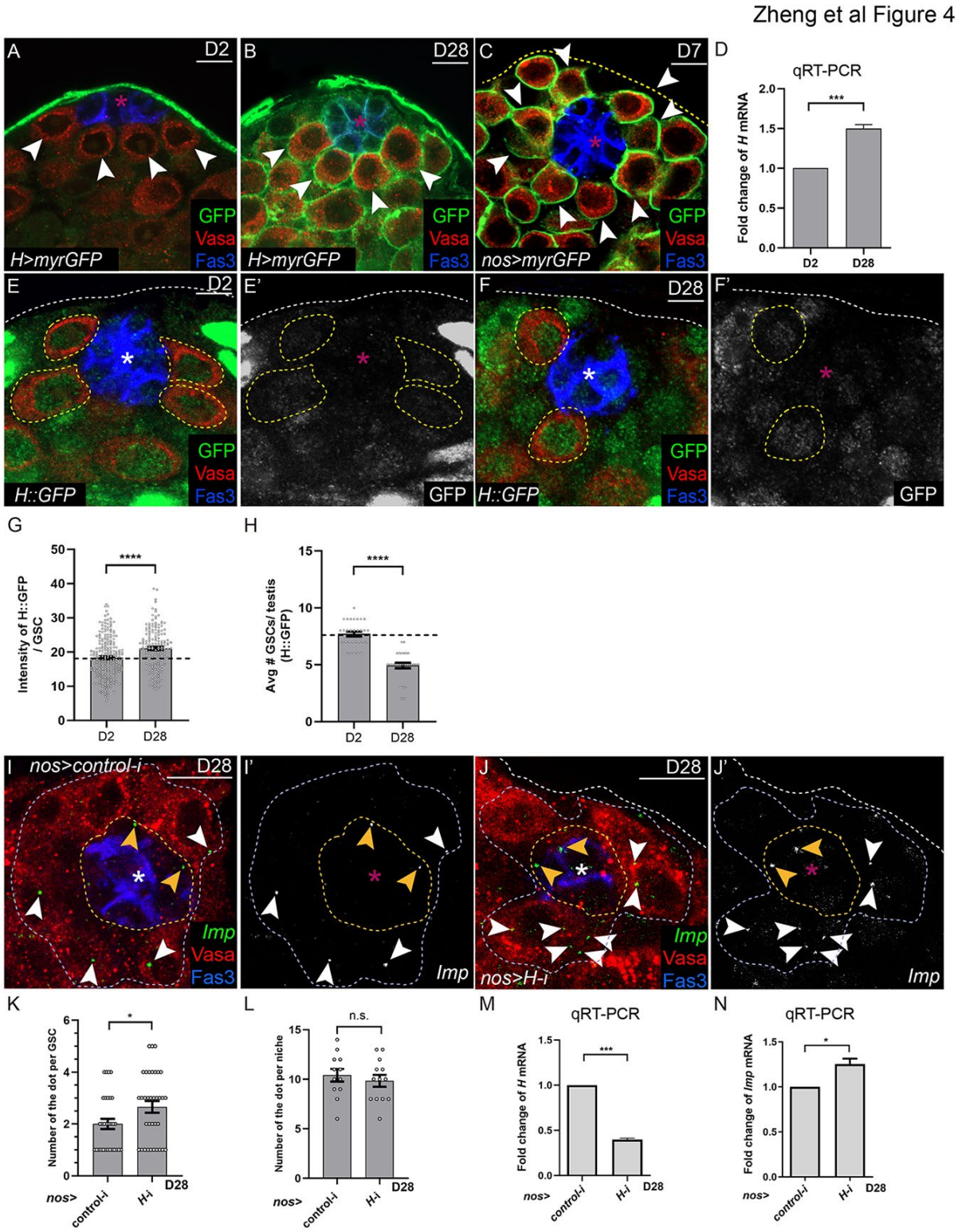

Figure 4. H is upregulated during aging and suppresses *Imp*.

(A–C) Confocal images of myristoylated GFP (myrGFP, green) in D2 (A) and D28 (B) *H>myrGFP* testes, and *nos>myrGFP* testes at D7 (C). Arrowheads indicate GSCs.

684 (D) Graph showing the relative fold change of *H* mRNA in D2 and D28 testes, measured by
685 qRT-PCR.
686 (E–H) Confocal images of H::GFP (green) in D2 (E) and D28 (F) testes, quantified in G. Graph
687 in H shows the average number of GSCs in D2 and D28 H::GFP testes. Dashed lines in E, F
688 indicate GSCs.
689 (I–L) RNA-FISH for *Imp* mRNA (green) in D28 *nos>control-i* (I) or *nos>H-i* (J) testes,
690 quantified in K for GSCs and in L for niche cells. Blue and yellow dashed lines circumscribes
691 the niche and GSCs, respectively. Arrowheads indicate *Imp* mRNA puncta.
692 (M, N) qRT-PCR analysis of *H* (M) or *Imp* (N) transcripts in D28 *nos>control-i* or *nos>H-i*
693 testes.
694 Asterisks in indicate the niche. Vasa labels germ cells; Fas3 labels niche cells.
695 Scale bars = 10 μm.
696 In G, H, K, L, M, and N, error bars represent SEM. * $P \leq 0.05$; *** $P \leq 0.001$; **** $P \leq$
697 0.0001 as assessed by Student's t-test.
698
699
700
701
702

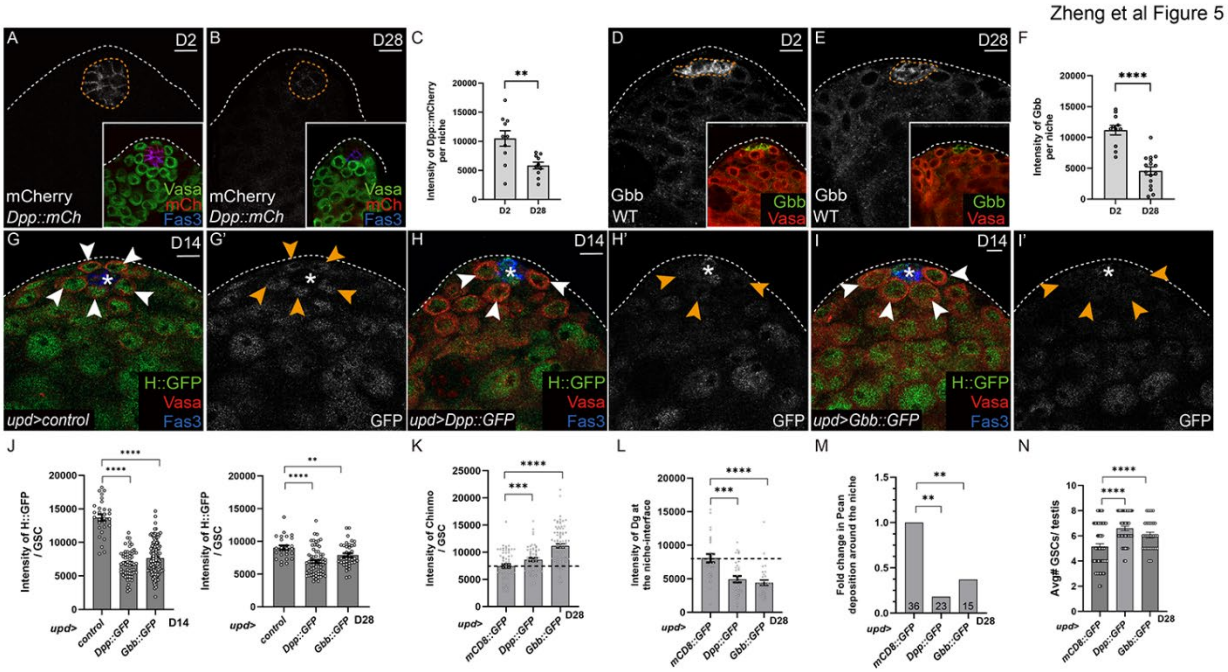

Figure 5. Overexpression of BMPs suppresses H and age-related phenotypes of the testis.

(A-F) Confocal images of Dpp::mCherry (abbreviated Dpp::mCh, white, A and B) and Gbb (white, D and E) in D2 (A, D) and D28 (B, E) testes, quantified in C for Dpp::mCherry and in G for Gbb. Orange dashed lines indicate the level of Dpp::mCherry and Gbb in niche cells.

(G–H) Confocal images of H::GFP (green) in D14 testes in *upd>+* (control, G), *upd>Dpp::GFP* (H), or *upd>Gbb::GFP* (I).

(J) Graph showing intensity of H::GFP per GSC in D14 (left) vs D28 (right) testes.

(K-N) Graph showing intensity of Chinmo (K) per GSC and Dg (L) at GSC-niche interface, the fold change in Pcan surrounding the niche (M), and the average total number of GSCs (N) in D28 testes in *upd>mCD8-GFP*, *upd>Dpp::GFP*, or *upd>Gbb::GFP*.

Asterisks in indicate the niche. Vasa labels germ cells; Fas3 labels niche cells.

Scale bars = 10 µm.

In C, F, J, K, L and N, error bars represent SEM. * $P \leq 0.05$; ** $P \leq 0.01$; *** $P \leq 0.001$; **** $P \leq 0.0001$ as assessed by Student's t-test for C, F, J, K, L and N, and by χ^2 test in M.

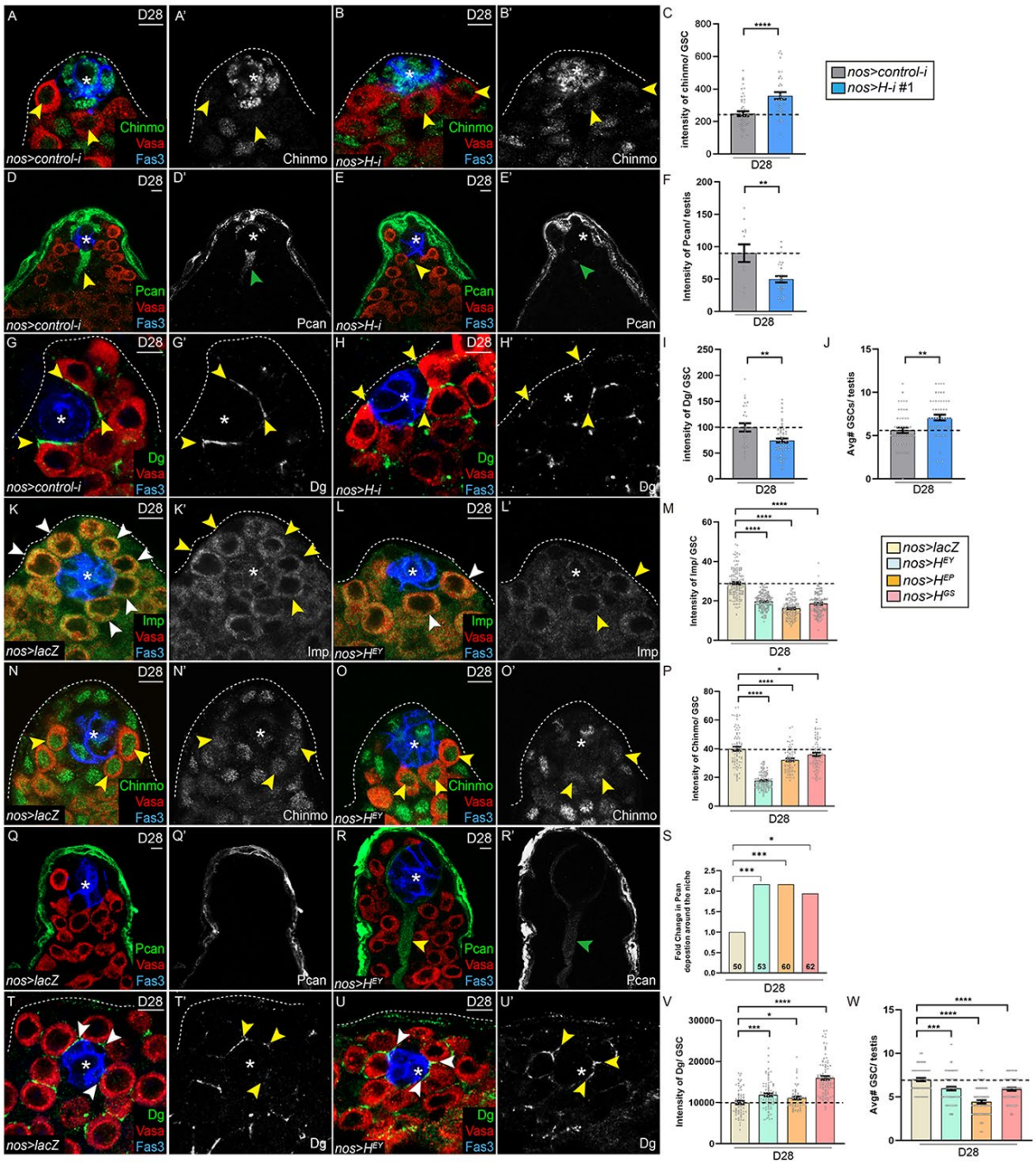

Figure 6. Hairless negatively regulates aging of the testis stem cell niche

(A-J) Confocal image of Chinmo (green, A, B), Pcan (green, D, E) or Dg (green, G, H) in D28 *nos>control-i* (A, D, G) or *nos>H-i* testes (B, E, H), quantified in C, F, I, respectively. Arrowheads indicate Chinmo in GSCs (A, B); ectopic Pcan surrounding the niche (D, E), or Dg at the GSC-niche interface (G, H). Graph in J shows the average number of GSCs in D28 indicated genotype testes.

726 (K-W) Confocal image of Imp (green, K, L), Chinmo (green, N, O), Pcan (green, Q, R), or Dg
727 (green, T, U) in D28 *nos>lacZ* (K, N, Q, T) or *nos>H*^{EY} testes (L, O, R, U), quantified in M, P,
728 S, V, respectively. Arrowheads indicate Imp in GSCs (K, L), Chinmo in GSCs (N, O), ectopic
729 Pcan in the testis lumen (R), or Dg at the GSC-niche interface (T, U). Graph in W shows the
730 average number of GSCs in D28 indicated genotype testes.
731 Asterisks in indicate the niche. Vasa labels germ cells; Fas3 labels niche cells.
732 Scale bar = 10 μM
733 In C, F, I, J, M, P, V, and W, error bars represent SEM. * $P \leq 0.05$; ** $P \leq 0.01$; *** $P \leq 0.001$;
734 **** $P \leq 0.0001$ as assessed by Student's t-test in C, F, I, J, M, P, V, and W, and by χ^2 test in S.
735

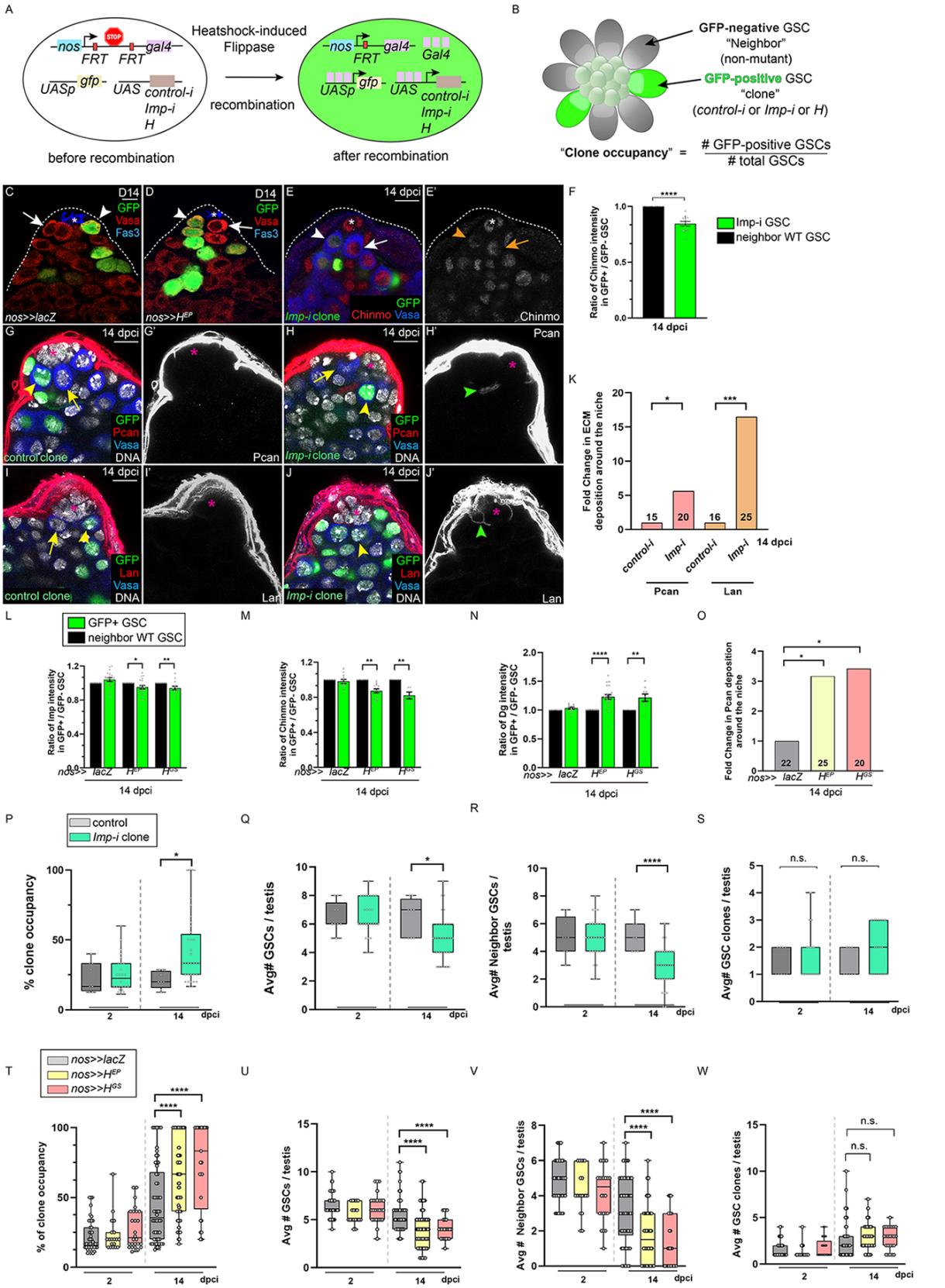
A
Heatshock-induced Flippase
recombination
before recombination
after recombination
B
GFP-negative GSC "Neighbor" (non-mutant)
GFP-positive GSC "clone" (control-i or Imp-i or H)
"Clone occupancy" = # GFP-positive GSCs / # total GSCs
nos>>lacZ
nos>>H^EP
Imp-i clone
control clone
Chinmo
Pcan
Lan
Ratio of Chinmo intensity in GFP+ / GFP- GSC
Imp-i GSC
neighbor WT GSC
Fold Change in ECM deposition around the niche
Fold Change in Pcan deposition around the niche
GFP+ GSC
Ratio of Imp intensity in GFP+ / GFP- GSC
Ratio of Dg intensity in GFP+ / GFP- GSC
control
% clone occupancy
Avg# GSCs / testis
Avg# Neighbor GSCs / testis
Avg# GSC clones / testis
nos>>lacZ
nos>>H^EP
nos>>H^GS
% of clone occupancy
Avg # GSCs / testis
Avg # Neighbor GSCs / testis
Avg # GSC clones / testis
14 dpci
dpci
n.s.

737 **Figure 7. *Imp*-deficient and H-overexpressing GSC clones gain a competitive advantage for**
738 **niche occupancy and evict non-mutant neighbors**
739 (A) Schematic of clone induction using the *nos* flip-out technique. The *nos* promoter drives the
740 expression of a cassette containing two *FRT* (Flippase Recognition Target) sites flanking a stop
741 codon and the *gal4* coding sequence on the same chromosome. A *UASp* promoter controls *gfp*,
742 and either *UAS-lacZ* (control) or *UAS-H* is also present in the GSC. Heat-shock induction of
743 Flippase (FLP) excises the intervening sequence between the *FRT* sites, removing the stop codon
744 and allowing Gal4 expression. As a result, Gal4 activates GFP and either LacZ or H from the
745 *UASp* or *UAS* promoter, leading to positively-labeled clones.
746 (B) Diagram illustrating the clone occupancy assay. In this testis, eight GSCs surround the niche.
747 Two GSCs are clones (either control or $Imp^{-/-}$) and are GFP-positive (green). The non-mutant
748 neighbor GSCs are GFP-negative. The occupancy of each clone is calculated by dividing the
749 number of GFP-positive GSCs by the total number of GSCs in each testis. In this example, the
750 clone occupancy is 25% (2 GSC clones/8 total GSCs).
751 (C, D) Confocal images of testes with GFP-positive *nos>>lacZ* GSC clones (C, arrowhead) or
752 *nos>>H* GSC clones (D, arrowhead) at 14 days post-clone induction (dpci). Arrows indicate
753 non-mutant neighboring GSCs.
754 (E-F) Confocal image of a testis harboring a GFP-positive $Imp^{-/-}$ GSC clone (arrowhead) at
755 14 dpci. The arrow indicates a GFP-negative non-mutant GSC neighbor. Graph in F shows the
756 ratio of Chinmo protein intensity in the GSC clone vs that in the non-mutant GSC for control
757 clones (black bar) and *Imp*-mutant clones (green bar). (G-K) Confocal images of Pcan (red, G,
758 H) and Lan (red, I, J) expression in the testis lumen with control GSC clones (G, I) or $Imp^{-/-}$ GSC
759 clones (H, J), quantified in K. Green arrowheads mark ectopic Pcan (H) or ectopic Lan (J) near
760 the niche. The total number of analyzed testes are indicated in each bar.
761 (L-O) Graph showing the ratio of Imp (L), Chinmo (M) or Dg (N) protein at the niche-GSC
762 interface in GSC clones (*i.e.*, *nos>>lacZ*, $nos>>H^{EP}$, or $nos>H^{GS}$ GSC clones (green bar)) to
763 neighbor GSCs (black bar) at 14 dpci.
764 (O) Graph quantifying the fold change Pcan surrounding the niche when *nos>>lacZ* GSC clones
765 (first bar), $nos>>H^{EP}$ GSC clones (second bar), or $nos>>H^{GS}$ GSC clones (third bar) are present.
766 The number of testes analyzed are indicated in each bar.
767 (P-S) Box-and-whisker plots depicting (P) clone occupancy, (Q) average total number of GSCs,

768 (R) average number of non-mutant GSC neighbors, and (S) average number of GSC clones in
769 testes containing control (gray bars) or *Imp*$^{-/-}$ (green bars) GSC clones at 2 and 14 dpci.
770 (T-W) Box and whisker plots showing clone occupancy (T), average total number of GSCs (U),
771 average number of non-mutant GSC neighbors (V), and average numbers of GSC clones (W) in
772 testes with control *nos>>lacZ* GSC clones (gray bars), with *nos>>H*^{EP} GSC clones (yellow bar),
773 or with *nos>>H*^{GS} GSC clones (pink bar) at 2 and 14 dpci.
774 Asterisks in indicate the niche. DAPI labels DNA; Vasa labels germ cells; Fas3 labels niche
775 cells.
776 Scale bars = 10 μm.
777 In F, L-N, P-W, error bars represent SEM. * $P \leq 0.05$, ** $P \leq 0.01$, *** $P \leq 0.001$, ****
778 $P \leq 0.0001$ by Student's t-test for F, L-N, P-W and by χ^2 test for K, O.

References

1. Morrison, S.J., and Spradling, A.C. (2008). Stem cells and niches: mechanisms that promote stem cell maintenance throughout life. Cell *132*, 598-611. 10.1016/j.cell.2008.01.038.
2. Brunet, A., Goodell, M.A., and Rando, T.A. (2023). Ageing and rejuvenation of tissue stem cells and their niches. Nature reviews. Molecular cell biology *24*, 45-62. 10.1038/s41580-022-00510-w.
3. Oh, J., Lee, Y.D., and Wagers, A.J. (2014). Stem cell aging: mechanisms, regulators and therapeutic opportunities. Nature medicine *20*, 870-880. 10.1038/nm.3651.
4. Harris, I.D., Fronczak, C., Roth, L., and Meacham, R.B. (2011). Fertility and the aging male. Rev Urol *13*, e184-190.
5. Khandwala, Y.S., Zhang, C.A., Lu, Y., and Eisenberg, M.L. (2017). The age of fathers in the USA is rising: an analysis of 168 867 480 births from 1972 to 2015. Hum Reprod *32*, 2110-2116. 10.1093/humrep/dex267.
6. Johnson, L., Zane, R.S., Petty, C.S., and Neaves, W.B. (1984). Quantification of the human Sertoli cell population: its distribution, relation to germ cell numbers, and age-related decline. Biology of reproduction *31*, 785-795. 10.1095/biolreprod31.4.785.
7. Paniagua, R., Nistal, M., Amat, P., Rodriguez, M.C., and Martin, A. (1987). Seminiferous tubule involution in elderly men. Biology of reproduction *36*, 939-947. 10.1095/biolreprod36.4.939.
8. Pohl, E., Hoffken, V., Schlatt, S., Kliesch, S., Gromoll, J., and Wistuba, J. (2019). Ageing in men with normal spermatogenesis alters spermatogonial dynamics and nuclear morphology in Sertoli cells. Andrology *7*, 827-839. 10.1111/andr.12665.
9. Buchwalter, A., and Hetzer, M.W. (2017). Nucleolar expansion and elevated protein translation in premature aging. Nature communications *8*, 328. 10.1038/s41467-017-00322-z.
10. Ryu, B.Y., Orwig, K.E., Oatley, J.M., Avarbock, M.R., and Brinster, R.L. (2006). Effects of aging and niche microenvironment on spermatogonial stem cell self-renewal. Stem cells (Dayton, Ohio) *24*, 1505-1511. 10.1634/stemcells.2005-0580.
11. Sato, T., Katagiri, K., Yokonishi, T., Kubota, Y., Inoue, K., Ogonuki, N., Matoba, S., Ogura, A., and Ogawa, T. (2011). In vitro production of fertile sperm from murine spermatogonial stem cell lines. Nature communications *2*, 472. 10.1038/ncomms1478.
12. Liggett, L.A., and DeGregori, J. (2017). Changing mutational and adaptive landscapes and the genesis of cancer. Biochim Biophys Acta Rev Cancer *1867*, 84-94. 10.1016/j.bbcan.2017.01.005.
13. Florez, M.A., Tran, B.T., Wathan, T.K., DeGregori, J., Pietras, E.M., and King, K.Y. (2022). Clonal hematopoiesis: Mutation-specific adaptation to environmental change. Cell stem cell *29*, 882-904. 10.1016/j.stem.2022.05.006.
14. Jaiswal, S., and Ebert, B.L. (2019). Clonal hematopoiesis in human aging and disease. Science (New York, N.Y *366*. 10.1126/science.aan4673.
15. Snippert, H.J., Schepers, A.G., van Es, J.H., Simons, B.D., and Clevers, H. (2014). Biased competition between Lgr5 intestinal stem cells driven by oncogenic mutation induces clonal expansion. EMBO reports *15*, 62-69. 10.1002/embr.201337799.
16. Snippert, H.J., van der Flier, L.G., Sato, T., van Es, J.H., van den Born, M., Kroon-Veenboer, C., Barker, N., Klein, A.M., van Rheenen, J., Simons, B.D., and Clevers, H.

(2010). Intestinal crypt homeostasis results from neutral competition between symmetrically dividing Lgr5 stem cells. Cell *143*, 134-144.

17. Lopez-Garcia, C., Klein, A.M., Simons, B.D., and Winton, D.J. (2010). Intestinal stem cell replacement follows a pattern of neutral drift. Science (New York, N.Y *330*, 822-825. 10.1126/science.1196236.
18. Amoyel, M., Simons, B.D., and Bach, E.A. (2014). Neutral competition of stem cells is skewed by proliferative changes downstream of Hh and Hpo. The EMBO journal *33*, 2295-2313. 10.15252/embj.201387500.
19. Vermeulen, L., Morrissey, E., van der Heijden, M., Nicholson, A.M., Sottoriva, A., Buczacki, S., Kemp, R., Tavare, S., and Winton, D.J. (2013). Defining stem cell dynamics in models of intestinal tumor initiation. Science (New York, N.Y *342*, 995-998. 10.1126/science.1243148.
20. van Neerven, S.M., de Groot, N.E., Nijman, L.E., Scicluna, B.P., van Driel, M.S., Lecca, M.C., Warmerdam, D.O., Kakkar, V., Moreno, L.F., Vieira Braga, F.A., et al. (2021). Apc-mutant cells act as supercompetitors in intestinal tumour initiation. Nature *594*, 436-441. 10.1038/s41586-021-03558-4.
21. Flanagan, D.J., Pentinmikko, N., Luopajarvi, K., Willis, N.J., Gilroy, K., Raven, A.P., McGarry, L., Englund, J.I., Webb, A.T., Scharaw, S., et al. (2021). NOTUM from Apc-mutant cells biases clonal competition to initiate cancer. Nature *594*, 430-435. 10.1038/s41586-021-03525-z.
22. Herms, A., Colom, B., Piedrafita, G., Kalogeropoulou, A., Banerjee, U., King, C., Abby, E., Murai, K., Caseda, I., Fernandez-Antoran, D., et al. (2024). Organismal metabolism regulates the expansion of oncogenic PIK3CA mutant clones in normal esophagus. Nature genetics *56*, 2144-2157. 10.1038/s41588-024-01891-8.
23. Colom, B., Herms, A., Hall, M.W.J., Dentro, S.C., King, C., Sood, R.K., Alcolea, M.P., Piedrafita, G., Fernandez-Antoran, D., Ong, S.H., et al. (2021). Mutant clones in normal epithelium outcompete and eliminate emerging tumours. Nature *598*, 510-514. 10.1038/s41586-021-03965-7.
24. Martincorena, I., Fowler, J.C., Wabik, A., Lawson, A.R.J., Abascal, F., Hall, M.W.J., Cagan, A., Murai, K., Mahbubani, K., Stratton, M.R., et al. (2018). Somatic mutant clones colonize the human esophagus with age. Science (New York, N.Y *362*, 911-917. 10.1126/science.aau3879.
25. Roan, H.Y., Tseng, T.L., and Chen, C.H. (2021). Whole-body clonal mapping identifies giant dominant clones in zebrafish skin epidermis. Development (Cambridge, England) *148*. 10.1242/dev.199669.
26. Goriely, A., and Wilkie, A.O. (2012). Paternal age effect mutations and selfish spermatogonial selection: causes and consequences for human disease. Am J Hum Genet *90*, 175-200. 10.1016/j.ajhg.2011.12.017.
27. Wood, K.A., and Goriely, A. (2022). The impact of paternal age on new mutations and disease in the next generation. Fertility and sterility *118*, 1001-1012. 10.1016/j.fertnstert.2022.10.017.
28. Hodge, R.A., and Bach, E.A. (2024). Mechanisms of Germline Stem Cell Competition across Species. Life (Basel) *14*. 10.3390/life14101251.
29. Wallenfang, M.R., Nayak, R., and DiNardo, S. (2006). Dynamics of the male germline stem cell population during aging of Drosophila melanogaster. Aging cell *5*, 297-304. 10.1111/j.1474-9726.2006.00221.x.

870 30. Boyle, M., Wong, C., Rocha, M., and Jones, D.L. (2007). Decline in self-renewal factors
871 contributes to aging of the stem cell niche in the Drosophila testis. Cell stem cell *1*, 470-
872 478. 10.1016/j.stem.2007.08.002.
873 31. Toledano, H., D'Alterio, C., Czech, B., Levine, E., and Jones, D.L. (2012). The let-7-Imp
874 axis regulates ageing of the Drosophila testis stem-cell niche. Nature *485*, 605-610.
875 10.1038/nature11061.
876 32. Herrera, S.C., Sainz de la Maza, D., Grmai, L., Margolis, S., Plessel, R., Burel, M.,
877 O'Connor, M., Amoyel, M., and Bach, E.A. (2021). Proliferative stem cells maintain
878 quiescence of their niche by secreting the Activin inhibitor Follistatin. Dev Cell *56*, 2284-
879 2294 e2286. 10.1016/j.devcel.2021.07.010.
880 33. Tseng, C.Y., Burel, M., Cammer, M., Harsh, S., Flaherty, M.S., Baumgartner, S., and
881 Bach, E.A. (2022). chinmo-mutant spermatogonial stem cells cause mitotic drive by
882 evicting non-mutant neighbors from the niche. Dev Cell *57*, 80-94 e87.
883 10.1016/j.devcel.2021.12.004.
884 34. Greenspan, L.J., de Cuevas, M., and Matunis, E. (2015). Genetics of gonadal stem cell
885 renewal. Annual review of cell and developmental biology *31*, 291-315.
886 10.1146/annurev-cellbio-100913-013344.
887 35. Leatherman, J.L., and Dinardo, S. (2008). Zfh-1 controls somatic stem cell self-renewal
888 in the Drosophila testis and nonautonomously influences germline stem cell self-renewal.
889 Cell stem cell *3*, 44-54.
890 36. Leatherman, J.L., and Dinardo, S. (2010). Germline self-renewal requires cyst stem cells
891 and stat regulates niche adhesion in Drosophila testes. Nature cell biology *12*, 806-811.
892 37. Tulina, N., and Matunis, E. (2001). Control of stem cell self-renewal in Drosophila
893 spermatogenesis by JAK-STAT signaling. Science (New York, N.Y *294*, 2546-2549.
894 38. Kiger, A.A., Jones, D.L., Schulz, C., Rogers, M.B., and Fuller, M.T. (2001). Stem cell
895 self-renewal specified by JAK-STAT activation in response to a support cell cue. Science
896 (New York, N.Y *294*, 2542-2545.
897 39. Kawase, E., Wong, M.D., Ding, B.C., and Xie, T. (2004). Gbb/Bmp signaling is essential
898 for maintaining germline stem cells and for repressing bam transcription in the
899 Drosophila testis. Development (Cambridge, England) *131*, 1365-1375.
900 40. Shivdasani, A.A., and Ingham, P.W. (2003). Regulation of stem cell maintenance and
901 transit amplifying cell proliferation by tgf-beta signaling in Drosophila spermatogenesis.
902 Curr Biol *13*, 2065-2072.
903 41. Inaba, M., Buszczak, M., and Yamashita, Y.M. (2015). Nanotubes mediate niche-stem-
904 cell signalling in the Drosophila testis. Nature. 10.1038/nature14602.
905 42. Wu, Y.C., Chen, C.H., Mercer, A., and Sokol, N.S. (2012). Let-7-complex microRNAs
906 regulate the temporal identity of Drosophila mushroom body neurons via chinmo. Dev
907 Cell *23*, 202-209. 10.1016/j.devcel.2012.05.013.
908 43. Yang, L., Chen, D., Duan, R., Xia, L., Wang, J., Qurashi, A., Jin, P., and Chen, D.
909 (2007). Argonaute 1 regulates the fate of germline stem cells in Drosophila. Development
910 (Cambridge, England) *134*, 4265-4272. 10.1242/dev.009159.
911 44. Flaherty, M.S., Salis, P., Evans, C.J., Ekas, L.A., Marouf, A., Zavadil, J., Banerjee, U.,
912 and Bach, E.A. (2010). chinmo is a functional effector of the JAK/STAT pathway that
913 regulates eye development, tumor formation, and stem cell self-renewal in Drosophila.
914 Dev Cell *18*, 556-568. 10.1016/j.devcel.2010.02.006.

45. Liu, Z., Yang, C.P., Sugino, K., Fu, C.C., Liu, L.Y., Yao, X., Lee, L.P., and Lee, T. (2015). Opposing intrinsic temporal gradients guide neural stem cell production of varied neuronal fates. Science (New York, N.Y *350*, 317-320. 10.1126/science.aad1886.
46. Narbonne-Reveau, K., Lanet, E., Dillard, C., Foppolo, S., Chen, C.H., Parrinello, H., Rialle, S., Sokol, N.S., and Maurange, C. (2016). Neural stem cell-encoded temporal patterning delineates an early window of malignant susceptibility in Drosophila. eLife *5*. 10.7554/eLife.13463.
47. Muller, D., Kugler, S.J., Preiss, A., Maier, D., and Nagel, A.C. (2005). Genetic modifier screens on Hairless gain-of-function phenotypes reveal genes involved in cell differentiation, cell growth and apoptosis in Drosophila melanogaster. Genetics *171*, 1137-1152. 10.1534/genetics.105.044453.
48. Mundorf, J., Donohoe, C.D., McClure, C.D., Southall, T.D., and Uhlirova, M. (2019). Ets21c Governs Tissue Renewal, Stress Tolerance, and Aging in the Drosophila Intestine. Cell reports *27*, 3019-3033 e3015. 10.1016/j.celrep.2019.05.025.
49. Li, H., Janssens, J., De Waegeneer, M., Kolluru, S.S., Davie, K., Gardeux, V., Saelens, W., David, F.P.A., Brbic, M., Spanier, K., et al. (2022). Fly Cell Atlas: A single-nucleus transcriptomic atlas of the adult fruit fly. Science (New York, N.Y *375*, eabk2432. 10.1126/science.abk2432.
50. Maier, D. (2006). Hairless: the ignored antagonist of the Notch signalling pathway. Hereditas *143*, 212-221. 10.1111/j.2007.0018-0661.01971.x.
51. Nagel, A.C., Krejci, A., Tenin, G., Bravo-Patino, A., Bray, S., Maier, D., and Preiss, A. (2005). Hairless-mediated repression of notch target genes requires the combined activity of Groucho and CtBP corepressors. Molecular and cellular biology *25*, 10433-10441. 10.1128/MCB.25.23.10433-10441.2005.
52. Barolo, S., Stone, T., Bang, A.G., and Posakony, J.W. (2002). Default repression and Notch signaling: Hairless acts as an adaptor to recruit the corepressors Groucho and dCtBP to Suppressor of Hairless. Genes & development *16*, 1964-1976. 10.1101/gad.987402.
53. Shyu, L.F., Sun, J., Chung, H.M., Huang, Y.C., and Deng, W.M. (2009). Notch signaling and developmental cell-cycle arrest in Drosophila polar follicle cells. Molecular biology of the cell *20*, 5064-5073. 10.1091/mbc.e09-01-0004.
54. Lee, T., and Luo, L. (1999). Mosaic analysis with a repressible cell marker for studies of gene function in neuronal morphogenesis. Neuron *22*, 451-461.
55. Ma, X., Wang, S., Do, T., Song, X., Inaba, M., Nishimoto, Y., Liu, L.P., Gao, Y., Mao, Y., Li, H., et al. (2014). Piwi is required in multiple cell types to control germline stem cell lineage development in the Drosophila ovary. PloS one *9*, e90267. 10.1371/journal.pone.0090267.
56. Zhao, R., Xuan, Y., Li, X., and Xi, R. (2008). Age-related changes of germline stem cell activity, niche signaling activity and egg production in Drosophila. Aging cell *7*, 344-354. 10.1111/j.1474-9726.2008.00379.x.
57. Yousef, H., Morgenthaler, A., Schlesinger, C., Bugaj, L., Conboy, I.M., and Schaffer, D.V. (2015). Age-Associated Increase in BMP Signaling Inhibits Hippocampal Neurogenesis. Stem cells (Dayton, Ohio) *33*, 1577-1588. 10.1002/stem.1943.
58. Valletta, S., Thomas, A., Meng, Y., Ren, X., Drissen, R., Sengul, H., Di Genua, C., and Nerlov, C. (2020). Micro-environmental sensing by bone marrow stroma identifies IL-6

960 and TGFbeta1 as regulators of hematopoietic ageing. Nature communications *11*, 4075.
961 10.1038/s41467-020-17942-7.
962 59. Egerman, M.A., Cadena, S.M., Gilbert, J.A., Meyer, A., Nelson, H.N., Swalley, S.E.,
963 Mallozzi, C., Jacobi, C., Jennings, L.L., Clay, I., et al. (2015). GDF11 Increases with Age
964 and Inhibits Skeletal Muscle Regeneration. Cell metabolism *22*, 164-174.
965 10.1016/j.cmet.2015.05.010.
966 60. Johannes, B., and Preiss, A. (2002). Wing vein formation in Drosophila melanogaster:
967 hairless is involved in the cross-talk between Notch and EGF signaling pathways.
968 Mechanisms of development *115*, 3-14. 10.1016/s0925-4773(02)00083-7.
969 61. Song, X., Wong, M.D., Kawase, E., Xi, R., Ding, B.C., McCarthy, J.J., and Xie, T.
970 (2004). Bmp signals from niche cells directly repress transcription of a differentiation-
971 promoting gene, bag of marbles, in germline stem cells in the Drosophila ovary.
972 Development (Cambridge, England) *131*, 1353-1364. 10.1242/dev.01026.
973 62. Suo, M., Rommelfanger, M.K., Chen, Y., Amro, E.M., Han, B., Chen, Z., Szafranski, K.,
974 Chakkarappan, S.R., Boehm, B.O., MacLean, A.L., and Rudolph, K.L. (2022). Age-
975 dependent effects of Igf2bp2 on gene regulation, function, and aging of hematopoietic
976 stem cells in mice. Blood *139*, 2653-2665. 10.1182/blood.2021012197.
977 63. Van Doren, M., Williamson, A.L., and Lehmann, R. (1998). Regulation of zygotic gene
978 expression in Drosophila primordial germ cells. Curr Biol *8*, 243-246.
979 64. Ekas, L.A., Baeg, G.H., Flaherty, M.S., Ayala-Camargo, A., and Bach, E.A. (2006).
980 JAK/STAT signaling promotes regional specification by negatively regulating wingless
981 expression in Drosophila. Development (Cambridge, England) *133*, 4721-4729.
982 10.1242/dev.02675.
983 65. Baksa, K., Parke, T., Dobens, L.L., and Dearolf, C.R. (2002). The Drosophila STAT
984 protein, stat92E, regulates follicle cell differentiation during oogenesis. Developmental
985 biology *243*, 166-175. 10.1006/dbio.2001.0539.
986 66. Silver, D.L., and Montell, D.J. (2001). Paracrine signaling through the JAK/STAT
987 pathway activates invasive behavior of ovarian epithelial cells in Drosophila. Cell *107*,
988 831-841.
989 67. Li, M.A., Alls, J.D., Avancini, R.M., Koo, K., and Godt, D. (2003). The large Maf factor
990 Traffic Jam controls gonad morphogenesis in Drosophila. Nature cell biology *5*, 994-
991 1000. 10.1038/ncb1058.
992 68. Zhu, S., Lin, S., Kao, C.F., Awasaki, T., Chiang, A.S., and Lee, T. (2006). Gradients of
993 the Drosophila Chinmo BTB-zinc finger protein govern neuronal temporal identity. Cell
994 *127*, 409-422.
995 69. Xu, T., and Rubin, G.M. (1993). Analysis of genetic mosaics in developing and adult
996 Drosophila tissues. Development (Cambridge, England) *117*, 1223-1237.
997 70. Brand, A.H., and Perrimon, N. (1993). Targeted gene expression as a means of altering
998 cell fates and generating dominant phenotypes. Development (Cambridge, England) *118*,
999 401-415.
1000 71. McGuire, S.E., Mao, Z., and Davis, R.L. (2004). Spatiotemporal gene expression
1001 targeting with the TARGET and gene-switch systems in Drosophila. Sci STKE *2004*, pl6.
1002 72. Zimmerman, S.G., Peters, N.C., Altaras, A.E., and Berg, C.A. (2013). Optimized RNA
1003 ISH, RNA FISH and protein-RNA double labeling (IF/FISH) in Drosophila ovaries.
1004 Nature protocols *8*, 2158-2179. 10.1038/nprot.2013.136.

1005

Supplementary Tables S1-S6

Supplementary figures and legends S1-S7

Table S1: GSC clone induction rate, related to Figs. 7, S1, S7

#	Figure	% testes with at least 1 GSC clone	Time point (dpci)	Average	n	P (statistical test)
1	S1D	control (*)	2	71.43%	28	
2	S1D	control (*)	7	33.33%	30	
3	S1D	control (*)	14	16.67%	24	
4	S1D	*AGO1*$^{-/-}$ (*)	2	52.94%	34	0.171 vs line 1 (χ^2-test)
5	S1D	*AGO1*$^{-/-}$ (*)	7	46.43%	56	0.406 vs line 2 (χ^2-test)
6	S1D	*AGO1*$^{-/-}$ (*)	14	00.00%	14	
7	7	control (^)	2	36.00%	18	
8	7	control (^)	14	18.51%	20	
9	7	*Imp-i* (^)	2	35.68%	26	0.826 vs line 7 (χ^2-test)
10	7	*Imp-i* (^)	14	31.81%	36	0.259 vs line 8 (χ^2-test)
11	S7	*nos>>control-i* (&)	2	60.00%	18	
12	S7	*nos>>control-i* (&)	14	45.65%	17	
13	S7	*nos>>Imp-i* (&)	2	58.06%	36	0.877 vs line 11 (χ^2-test)
14	S7	*nos>>Imp-i* (&)	14	60.86%	29	0.097 vs line 12 (χ^2-test)
15	7	*nos>>LacZ* (&)	2	63.77%	44	
16	7	*nos>>LacZ* (&)	14	41.89%	62	
17	7	*nos>>H*^{EP} (&)	2	46.51%	20	0.073 vs line15 (χ^2-test)
18	7	*nos>>H*^{EP} (&)	14	62.42%	93	0.171 vs line 16 (χ^2-test)
19	7	*nos>>H*^{GS} (&)	2	57.78%	26	0.521 vs line 15 (χ^2-test)
20	7	*nos>>H*^{GS} (&)	14	39.06%	25	0.406 vs line 16 (χ^2-test)

* Denotes GFP-negative GSC clones generated by FLP/FRT
^ Denotes GFP-positive GSC clones generated by MARCM
& Denotes GFP-positive GSC clones generated by *nos* flip-out

Table S2: Clone occupancy, GSC number, number of neighbor GSCs, and number of GSC clones (clones induced by MARCM), related to Fig. 7

	Figure	Label	Time point (dpci)	Average	SEM	n	P (statistical test)
		Clone occupancy					
1	7P	control	2	23.10%	±3.35	18	
2	7P	control	14	21.12%	±1.98	20	
3	7P	*Imp-i*	2	25.24%	±3.63	26	
4	7P	*Imp-i*	14	44.38%	±5.38	36	0.0199 vs line 2 (Student's t-test)
		Avg. number of GSCs					
5	7Q	control	2	6.56	±0.32	18	
6	7Q	control	14	6.50	±0.43	20	
7	7Q	*Imp-i*	2	6.54	±0.38	26	
8	7Q	*Imp-i*	14	5.06	±0.37	36	0.0233 vs line 6 (Student's t-test)
		Avg. number of neighbor GSCs					
9	7R	control	2	5.11	±0.43	18	
10	7R	control	14	5.13	±0.37	20	
11	7R	*Imp-i*	2	4.96	±0.42	26	
12	7R	*Imp-i*	14	2.91	±0.33	36	2.0×10^{-4} vs line 10 (Student's t-test)
		Avg. number of GSC clones					
13	7S	control	2	1.44	±0.17	18	
14	7S	control	14	1.38	±0.17	20	
15	7S	*Imp-i*	2	1.58	±0.20	25	0.52 vs line 13
16	7S	*Imp-i*	14	1.92	±0.30	36	0.1191 vs line 14

Table S3: Clone occupancy, GSC number, number of neighbor GSCs, and number of GSC clones (clones induced by *nos* flip-out), related to Fig. S7

	Figure	Label	Time point (dpci)	Average	SEM	n	P (statistical test)
		Clone occupancy					
1	S7F	*nos>>control-i*	2	22.21%	±2.74	18	
2	S7F	*nos>>control-i*	14	30.27%	±1.63	17	
3	S7F	*nos>>Imp-i*	2	36.82%	±3.64	36	
4	S7F	*nos>>Imp-i*	14	55.26%	±4.47	29	0.003 vs line 18 (Student's t-test)
		Avg. number of GSC					
5	S7G	*nos>>control-i*	2	6.67	±0.27	18	
6	S7G	*nos>>control-i*	14	7.11	±0.25	17	
7	S7G	*nos>>Imp-i*	2	5.65%	±0.19	36	
8	S7G	*nos>>Imp-i*	14	4.44%	±0.25	29	$3X10^4$ vs line 22 (Student's t-test)
		Avg. number of neighbor GSCs					
9	S7H	*nos>>control-i*	2	5.17	±0.27	18	
10	S7H	*nos>>control-i*	14	3.49	±0.26	17	
11	S7H	*Imp-i*	2	4.94	±0.26	36	
12	S7H	*Imp-i*	14	2.07	±0.23	29	2.0×10^{-4} vs line 10 (Student's t-test)
		Avg. number of GSC clone					
13	S7I	*nos>>control-i*	2	1.28	±0.13	18	
14	S7I	*nos>>control-i*	14	2.16	±0.22	17	
15	S7I	*nos>>Imp-i*	2	1.72	±0.21	36	0.0851 vs line 13
16	S7I	*nos>>Imp-i*	14	2.37	±0.23	29	0.5379 vs line 14

Table S4: Clone occupancy, GSC number, number of neighbor GSCs, and number of GSC clones (clones induced by *nos* flip-out), related to Fig. 7.

	Figure	Label	Time point (dpci)	Average	SEM	n	P (statistical test)
		Clone occupancy					
1	7T	*nos>>lacZ*	2	22.10%	±1.70	44	
2	7T	*nos>>lacZ*	14	41.86%	±3.67	62	
3	7T	*nos>>H^{EP}*	2	23.58%	±2.85	19	
4	7T	*nos>>H^{EP}*	14	63.92%	±2.90	93	$9X10^{-5}$ vs line 2 (Student's t-test)
5	7T	*nos>>H^{GS}*	2	27.63%	±2.76	26	
6	7T	*nos>>H^{GS}*	14	73.60%	±6.05	25	$2.7X10^{-4}$ vs line 2 (Student's t-test)
		Avg. number of GSCs					
7	7U	*nos>>lacZ*	2	6.45	±0.19	44	
8	7U	*nos>>lacZ*	14	5.17	±0.19	62	
9	7U	*nos>>H^{EP}*	2	5.63	±0.23	19	
10	7U	*nos>>H^{EP}*)	14	3.85	±0.19	93	$1X10^{-8}$ vs line 8 (Student's t-test)
11	7U	*nos>>H^{GS}*	2	6.27	±0.29	26	
12	7U	*nos>>H^{GS}*	14	4.08	±0.22	25	$7.3X10^{-6}$ vs line 8 (Student's t-test)
		Avg. number of neighbor GSCs					
13	7V	*nos>>lacZ*	2	4.72	±0.18	44	
14	7V	*nos>>lacZ*	14	3.18	±0.25	62	
15	7V	*nos>>H^{EP}*	2	4.31	±0.29	19	
16	7V	*nos>>H^{EP}*	14	1.67	±0.16	93	$3.14X10^{-6}$ vs line 14 (Student's t-test)
17	7V	*nos>>H^{GS}*	2	4.17	±0.30	26	
18	7V	*nos>>H^{GS}*	14	1.22	±0.29	25	$2.3X10^{-6}$ vs line 14 (Student's t-test)
		Avg. number of GSC clones					
19	7W	*nos>>lacZ*	2	1.66	±0.13	44	
20	7W	*nos>>lacZ*	14	2.04	±0.17	62	
21	7W	*nos>>H^{EP}*	2	1.32	±0.17	20	
22	7W	*nos>>H^{EP}*	14	2.42	±0.12	93	0.25 vs line 20
23	7W	*nos>>H^{GS}*	2	1.76	±0.19	26	
24	7W	*nos>>H^{GS}*	14	2.76	±0.24	25	0.54 vs line 20

Table 5: Genotypes in each figure

Figure	Full genotype	Abbreviation used in figure
1B-E, G-O	*w^{1118}*	WT
1E	*y, w/Y; nos-Gal4/+; UAS-lacZ/+*	*nos>lacZ*
1E	*y, w/ Y; nos-Gal4/+; UAS-chimmo^{HMS00036} RNA-i /+*	*nos>chinmo-i*
2A-F, I	*Oregon-R*	WT
2G-I	*y, w*	WT
2J-L	*P{PTT-un}Imp^{ZCL2884X}/Y*	*Imp::GFP #1*
2M, O, P	*w/Y; nos-Gal4/+; UAS-lacZ/+*	*nos>lacZ*
2N, O, P	*w/Y; nos-Gal4/+; UAS-Imp-HA/ +*	*nos>Imp*
3A, C, E, F, H	*w/Y; nos-Gal4/+; UAS-lacZ/+*	*nos>lacZ*
3B, D, E, G, H	*w/Y; nos-Gal4/+; UAS-Imp-HA/+*	*nos>Imp*
3I, M, N, R, S	*w/Y; nos-Gal4/UAS-lacZ; UAS-lacZ/+*	*nos>lacZ, lacZ*
3J, M, O, R, S	*w/Y; nos-Gal4/UAS-lacZ/+; UAS-chimmo^{HMS00036} RNA-i/+*	*nos>lacZ, chinmo-i*
3K, M, P, R, S	*w/Y; nos-Gal4/UAS-Imp-i ^{GL00660}; UAS-lacZ/+*	*nos>Imp-i, lacZ*
3L, M, Q-S	*w/Y; nos-Gal4/UAS-Imp-i ^{GL00660}; UAS-chinmo/+*	*nos>Imp-i, chinmo*
4A, B	*y, w/Y; H-Gal4/+; UASp-myr::GFP/+*	*H>myrGFP*
4C	*y, w/Y; nos-Gal4/+; UASp-myr::GFP/+*	*nos>myrGFP*
4D	*Oregon-R*	WT
4E-H	*w/Y; Hairless::GFP*	*H::GFP*
4I, K-N	*y, w/Y; nos-Gal4/+; UAS-control RNAi/+*	*nos>control-i*
4J-N	*y, w/Y; nos-Gal4/+; UAS-H^{HMS01182}RNAi/+*	*nos>H-i*
5A-C	*y, w/Y; Dpp::mCherry/+*	*Dpp::mCh*
5D-F	*y, w/Y*	WT

5G, J	*upd-Gal4, tubGal80^{ts}/Y*	*upd>control*
5K-N	*upd-Gal4, tubGal80^{ts}/Y; UAS-mCD8::GFP/+*	*upd>mCD8::GFP*
5K-N	*upd-Gal4, tubGal80^{ts}/Y; UAS-dpp::GFP/+*	*upd>Dpp::GFP*
5K-N	*upd-Gal4, tubGal80^{ts}/Y; UAS-Gbb::GFP/+*	*upd>Gbb::GFP*
6A, C, D, F, G, I, J	*y, w/Y; nos-Gal4/+; UAS-control RNAi/+*	*nos>control-i*
6B, C, E, F, H, I, J	*y, w/Y; nos-Gal4/+; UAS-H^{HMS01182}RNAi/+*	*nos>H-i*
6K, M, N, P, Q, S-W	*y, w/ Y; nos-Gal4/+; UAS-lacZ/ +*	*nos>lacZ*
6L, M, O, P, R, S, U-W	*y, w/ Y; nos-Gal4/+; UAS-H^{EY03696}/+*	*nos>H^{EY}*
6P, S, V, W	*y, w/ Y; nos-Gal4/+; UAS-H^{EP-211}/ +*	*nos>H^{EP}*
6P, S, V, W	*y, w/ Y; nos-Gal4/+; UAS-H^{GS11776}/ +*	*nos>H^{GS}*
7C, L-O, T-W	*y, w, hs-flp/Y; nos-FRT-GAL4-VP16-nos 3'UTR/UASp-gfp; UAS-lacZ/+*	*nos>>lacZ*
7D, L-O, T-W	*y, w, hs-flp/Y; nos-FRT-GAL4-VP16-nos-3'UTR/UASp-gfp; UAS-H^{EP-211}/ +*	*nos>>H^{EP}*
7E, F, H, J, K, P-S	*y, w, hs-flp^{122}, tub-Gal4, UAS-nls-GFP/Y; tub-Gal80, FRT^{40A}/FRT^{40A}; UAS-Imp^{GD9232}RNAi/+*	*Imp-i* clone
7F, G, I, K, P-S	*y, w, hs-flp^{122}, tub-Gal4, UAS-nls-GFP/Y; tub-Gal80, FRT^{40A}/FRT^{40A}*	control clone
7N, P-W	*y, w, hs-flp/Y; nos-mCherry-SV40-polyA-FRT-GAL4-VP16-nos 3'UTR/UASp-gfp; UAS-lacZ/+*	*nos>>lacZ*
7L-O, T-W	*y, w, hs-flp/Y; nos-FRT-GAL4-VP16-nos 3'UTR/UASp-gfp; UAS-H^{GS11776}/+*	*nos>>H^{GS}*
S1A, C	*y, w, hs-flp^{122}, tub-Gal4, UAS-nls-GFP/Y; FRT^{82B}, tub-Gal80/ FRT^{82B}, Dcr-1^{Q1147XA}*	*Dcr-1$^{-/-}$* clone
S1B-D	*y, w, hs-flp^{122}/Y; FRT^{42D}, ubi-GFP/ FRT^{42D}, AGO^{1k08121}*	*AGO1$^{-/-}$* clone
S1D	*y, w, hs-flp^{122}/Y; FRT^{42D}, ubi-GFP/FRT^{42D}*	control clone

S1E, F, I	*y, w/Y; nos-Gal4/+; UAS-control-RNAi/+*	*nos>control-i*
S1G, I	*y, w/Y; nos-Gal4/+; UAS-drosha^{HMS00064} RNAi/+*	*nos>drosha-i*
S1H, I	*y, w/Y; nos-Gal4/UAS-mCherry.mir-let7.sponge; UAS-mCherry.mir-let7.sponge/+*	*nos>mir-let7.sponge*
S1J, L	*+/Y; Stat92E^{F}, e/+*	*control*
S1K, L	*y, w/Y; tj-Gal4/UASp-3HA-Stat92E$^{FL\#5}$; Stat92E^{F}, e/Stat92E^{85c9}, ca, e*	*tj>HA-Stat92E; Stat92E$^{F/85c9}$*
S2A-C	*w*/Y; P{PTT-un}Imp^{ZCL2884X}*	*Imp::GFP$^{\#2}$*
S2D, E, G	*y, w/Y; nos-Gal4/+; UAS-lacZ/+*	*nos>lacZ*
S2F, G	*y, w/Y; nos-Gal4/+; UAS-Imp-HA/+*	*nos>Imp*
S3A, D, E, F, H, I	*y, w/Y; nos-Gal4/+; UAS-control-RNAi/+*	*nos>control-i*
S3B, D, H, I	*y, w/Y; nos-Gal4/+; UAS-Imp-i ^{GL00660}/+*	*nos>Imp-i$^{B\#38219}$*
S3C, D, G, H, I	*y, w/Y; nos-Gal4/+; UAS-Imp-i ^{GD9232}/+*	*nos>Imp-i$^{V\#20321}$*
S4A, D, G, I, J	*y, w/Y; nos-Gal4/+; UAS-control-RNAi/+*	*nos>control-i*
S4B, D	*y, w/Y; nos-Gal4/+; UAS-dicer1^{HMS00141} RNAi/+*	*nos>Dcr1-i*
S4C, D	*y, w/Y; nos-Gal4/+; UAS-drosha^{HMS00064} RNAi/+*	*nos>drosha-i*
S4E, F	*Oregon-R*	WT
S4H, I, J	*y, w/Y; nos-Gal4/UAS-syp^{GD9477} RNAi*	*nos>Syp-i*
S4K, M	*y, w/ Y; nos-Gal4/+; UAS-lacZ/+*	*nos>lacZ*
S4L, M	*y, w/ Y; nos-Gal4 /+; UAS-5'UTR-Chinmo-3'UTR/+*	*nos>chinmo*
S5A, E, G, H, J, K, M, N, P, Q	*y, w/ Y; nos-Gal4/+; UAS-control-RNAi/+*	*nos>control-i*
S5A	*y, w/Y; nos-Gal4/+; UAS-H^{HMS01182} RNAi/+*	*nos>H-i*
S5A	*y, w/Y; nos-Gal4/+; UAS-Ets21^{HMS01989} RNAi/+*	*nos>Ets21-i*
S5A	*y, w/Y; nos-Gal4/+; UAS-p53^{HMS02286} RNAi/+*	*nos>p53-i*

S5B, D	*Imp$^{MI05901\text{-}GFSTF.2}$/Y; nos-Gal4/+; UAS-control-RNAi/+*	*nos>control-i*
S5C, D	*Imp$^{MI05901\text{-}GFSTF.2}$/Y; nos-Gal4/+; UAS-H^{HMS01182} RNAi/+*	*nos>H-i*
S5F, G, I, J, L, M, O, P, Q	*y, w/Y; nos-Gal4/+; UAS-H^{JF02624} RNAi/+*	*nos>H-i#2*
S6A-C	*w/Y; Suppressor of Hairless (Su(H))::GFP*	*Su(H)::GFP*
S6D, F	*w*/Y; Notch responsive element (NRE)-GFP*	*NRE-GFP*
S6E, G	*w*/Y; Notch responsive element (NRE)-RFP*	*NRE-RFP*
S6H	*y, w/Y; nos-Gal4/NRE-GFP; UAS-control-RNAi/+*	*nos>control-i*
S6I	*y, w/Y; nos-Gal4/ NRE-GFP; UAS-H^{HMS01182} RNAi/+*	*nos>H-i*
S6J	*y, w/Y; nos-Gal4/NRE-RFP; UAS-control-RNAi/+*	*nos>control-i*
S6K	*y, w/Y; nos-Gal4/ NRE-RFP; UAS-H^{HMS01182} RNAi/+*	*nos>H-i*
S6L, N, O	*y, w/Y; nos-Gal4/ +; UAS-lacZ/+*	*nos>lacZ*
S6M-O	*y, w/Y; nos-Gal4/+; UAS-N^{ICD}/ +*	*nos>N^{ICD}*
S7A, C, E-I	*y, w, hs-flp/Y; nos-FRT-gal4-VP16-nos 3'UTR/UASp-GFP; UAS-control-RNAi/+*	*nos>>control-i*
S7B, D, E-I	*y, w, hs-flp/Y; nos-FRT-gal4-VP16-nos 3'UTR/UASp-GFP; UAS-Imp-i$^{B\#38219}$/+*	*nos>>Imp-i$^{B\#38219}$*
Table S1	*y, w, hs-flp^{122}/Y; FRT^{42D} ubi-GFP/FRT^{42D}*	control (*)
	y, w, hs-flp^{122}/Y; FRT^{42D} ubi-GFP/FRT^{42D} AGO1^{k08121}	*AGO1$^{-/-}$* (*)
	y, w, hs-flp^{122}, tub-Gal4, UAS-nls-GFP/Y; tub-Gal80, FRT^{40A}/FRT^{40A}	control (^)
	y, w, hs-flp^{122}, tub-Gal4, UAS-nls-GFP/Y; tub-Gal80, FRT^{40A}/FRT^{40A}; UAS-Imp^{GL00660} RNAi/+	*Imp-i* (^)

	y, w, hs-flp/Y; nos-FRT-gal4-VP16-nos 3'UTR/UASp-GFP; UAS-control-RNAi/+	*nos>>control-i* (&)
	y, w, hs-flp/Y; nos-FRT-gal4-VP16-nos 3'UTR/UASp-GFP; UAS-Imp-i^{GL00660} /+	*nos>>Imp-i* (&)
	y, w, hs-flp/Y; nos-FRT-gal4-VP16-nos 3'UTR/UASp-GFP; UAS-lacZ/+	*nos>>LacZ* (&)
	y, w, hs-flp/Y; nos-FRT-gal4-VP16-nos 3'UTR/UASp-GFP; UAS-H^{EP-211}/ +	*nos>>H^{EP}* (&)
	y, w, hs-flp/Y; nos-FRT-gal4-VP16-nos 3'UTR/UASp-GFP; UAS-H^{GS11776}/+	*nos>>H^{GS}* (&)
Table S2	*y, w, hs-flp^{122}, tub-Gal4, UAS-nls-GFP/Y; tub-Gal80, FRT^{40A}/FRT^{40A}*	control
	y, w, hs-flp^{122}, tub-Gal4, UAS-nls-GFP/ Y; tub-Gal80, FRT^{40A}/FRT^{40A}; UAS-Imp^{GL00660} RNAi/+	*Imp-i*
Table S3	*y, w, hs-flp/Y; nos-FRT-gal4-VP16-nos 3'UTR/UASp-GFP; UAS-control-RNAi/+*	*nos>>control-i*
	y, w, hs-flp/Y; nos-FRT-gal4-VP16-nos 3'UTR/UASp-GFP; UAS-Imp-i^{GL00660}/+	*nos>>Imp-i*
Table S4	*y, w, hs-flp/Y; nos-FRT-gal4-VP16-nos 3'UTR/UASp-GFP; UAS-lacZ/ +*	*nos>>LacZ*
	y, w, hs-flp/Y; nos-FRT-gal4-VP16-nos 3'UTR/UASp-GFP; UAS-H^{EP-211}/ +	*nos>>H^{EP}*
	y, w, hs-flp/Y; nos-FRT-gal4-VP16-nos 3'UTR/UASp-GFP; UAS-H^{GS11776}/+	*nos>>H^{GS}*

Table S6. Primers for real-time qRT-PCR and RNA-FISH, related to Figures 1, 2, 5.

	Figure	**Primer for real-time qPCR**	**Sequence 5'-3'**
1	1E	*chinmo*	F: TTATCCTGCGATGGCGTAGTA
2			R: ACAGATCGGCGAACTTCTTTG
3	2D 4N	*Imp*	F: CCTCACGGTTGAGTTGCTTGT
4		*Imp*	R: TTGATCACACTGCCCGTCAC
5	4D, M	*H*	F: CGACGTCTTCAGATCGCATTGG
6		*H*	R: CGAACTCGCGCAGGATTCTTTTC
7	Internal control	*Rpl19*	F: TGAAATCAACGAGATCGCTAACA
8		*Rpl19*	R: TGTTGTCGATACCCTTGGGC
9	Internal control	*Rpl32*	F: AGATCGTGAAGAAGCGCACC
10		*Rpl32*	R: GACGCACTCTGTTGTCGATACC
		Primer for *Imp* RNA probe for RNA-FISH	
11	2A, B, C; 4 I, J, K, L	*Imp*	F: GATCACTGTCAGCTCTATCAACG
		Imp	R: GAATAGTCCGATGATGTGCACTG

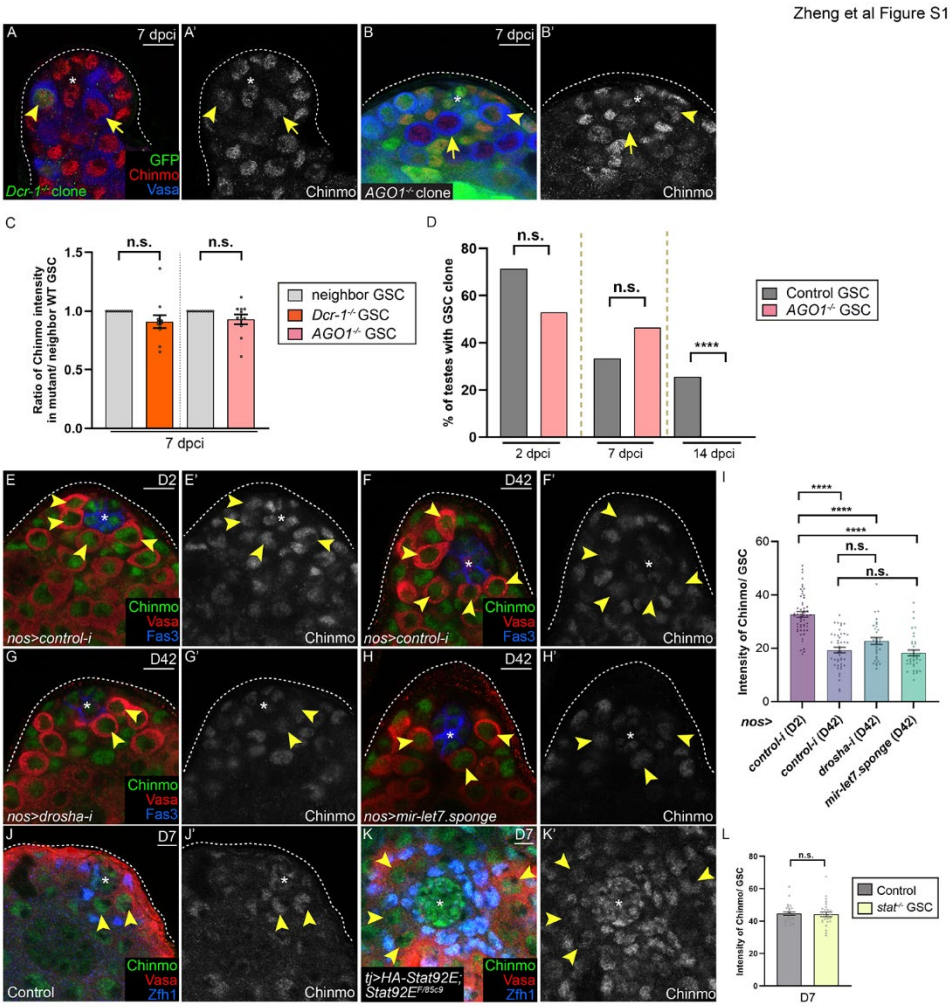

Figure S1. Chinmo is not regulated by the miRNA machinery in GSCs, related to Fig. 1

(A, B) Confocal images of Chinmo (red) in testes with (A) MARCM *Dcr-1*$^{-/-}$ GSC clones (A, arrowhead) or (B) GFP-negative *AGO1*$^{-/-}$ GSC clones (B, arrowhead) at 14 days post-clone induction (dpci). Arrows indicate non-mutant neighbor GSCs.

(C) Graph showing the ratio of Chinmo protein in *Dcr-1*$^{-/-}$ (orange bar) or *AGO1*$^{-/-}$ GSC clones (pink bar) compared to non-mutant neighbor GSCs (gray bars) per testis.

(D) Graph quantifying the percentage of testes harboring control (gray bars) or *AGO1*$^{-/-}$ (pink bars) GSC clones at 2, 7, and 14 dpci.

(E–I) Confocal images of Chinmo (green) in D2 (E) or D42 (F–H) *nos>control-i* (E, F), *nos>drosha-i* (G), or *nos>mir-let7.sponge* (H) testes, quantified in I.

(J-L) Confocal images of Chinmo protein (green) in control (*Stat92E*^{F}/+, J) or in STAT-deficient GSCs maintained by STAT-expressing, Tj-positive somatic support cells (*tj-Gal4/UASp-3HA-Stat92E*$^{FL\#5}$*; Stat92E*$^{F/85c9}$, K), quantified in L. Note in K the Vasa-positive GSC-like cells (arrowheads) are located 1 cell diameter's distance away from the niche. Arrowheads label GSCs in E-H, J and GSC-like cells in K.

Asterisks indicate the niche. Vasa marks germ cells and Fas3 marks niche cells. Zfh-1 labels CySCs and their immediate daughter cells.

Scale bars = 10 µm.

Error bars in C, I, L represent SEM. **** $P \leq 0.0001$; n.s. = not significant, as assessed by Student's t-test and by χ^2 test in D (see STAR Methods)

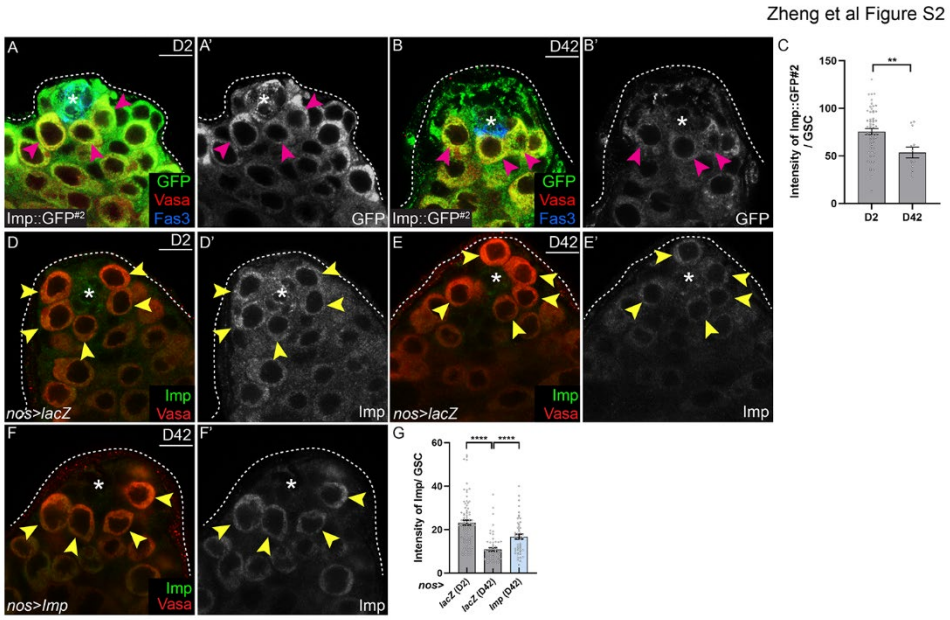

Figure S2. Imp is decreased in GSCs during aging, related to Fig. 2

(A–C) Confocal images of Imp::GFP #2 protein trap (green) in D2 (A) or D28 testes (B), quantified in C. Arrowheads indicate Imp::GFP #2 expression in GSCs.

(D–G) Confocal images of Imp protein (green) in D2 and D42 *nos>lacZ* (D, E) or D42 *nos>Imp* (F) testes, quantified in G. Arrowheads mark Imp expression in GSCs. Asterisks indicate niche cells. Vasa marks germ cells and Fas3 labels niche cells.

Scale bars = 10 µm.

Error bars in C, G represent SEM. **P $\leq$ 0.01: **** P $\leq$ 0.0001 by Student's t-test (see STAR Methods).

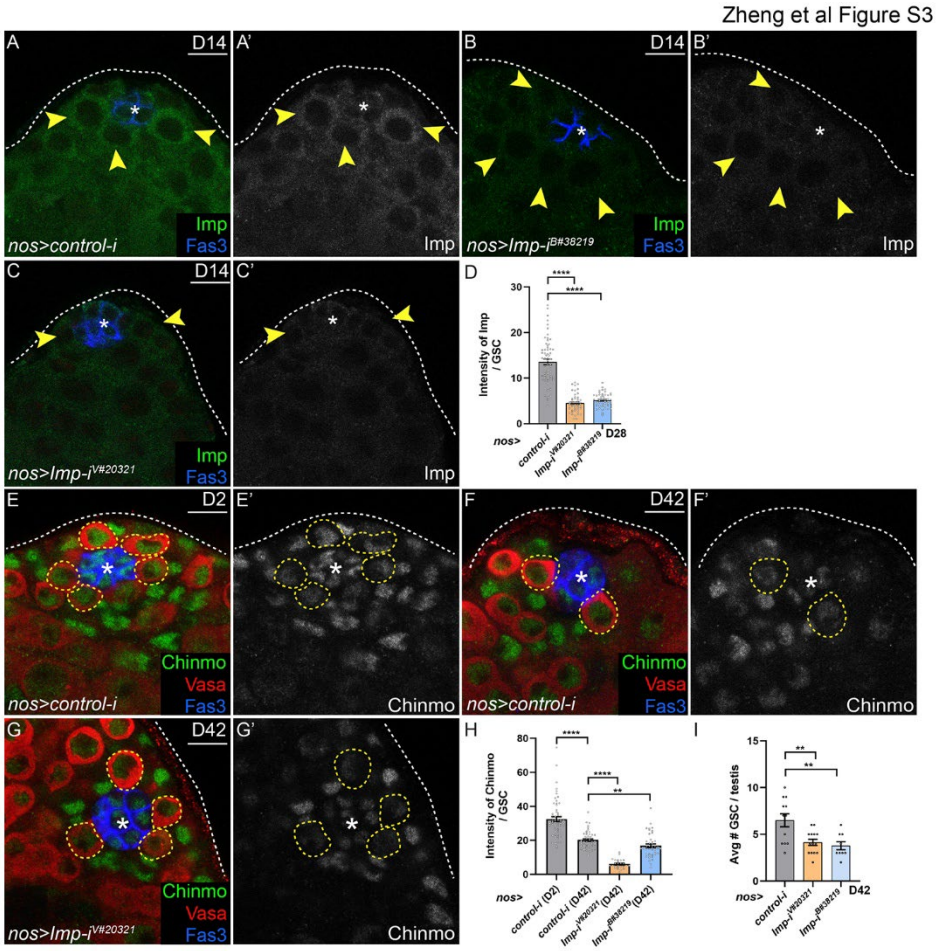

Figure S3. Imp RNAi efficiently depletes Imp, leading to reduced Chinmo and impaired GSC homeostasis, related to Fig. 3

(A–D) Confocal images of Imp protein (green) in D14 *nos>control-i* (A), *nos>Imp-i*$^{B\#38219}$ (B), or *nos>Imp-i*$^{V\#20321}$ (C) testes, quantified in D. Arrowheads indicate Imp expression in GSCs.

(E–H) Confocal images of Chinmo (green) in D2 or D42 *nos>control-i* testes (E, F), and D42 *nos>Imp-i*$^{V\#20321}$ (G) testes, quantified in H. Dashed lines indicate GSCs.

(I) Graph showing the number of GSCs in D2 or D42 *nos>control-i* (gray bar), D42 *nos>Imp-i*$^{B\#38219}$ (orange bar), or D42 *nos>Imp-i*$^{V\#20321}$ (blue bar) testes.

Asterisks indicate niche cells. Vasa marks germ cells and Fas3 labels niche cells.

Scale bars = 10 μm.

Error bars in H, Irepresent SEM. ** $P \leq 0.01$; ****; $P \leq 0.0001$ by Student's t-test (see STAR Methods).

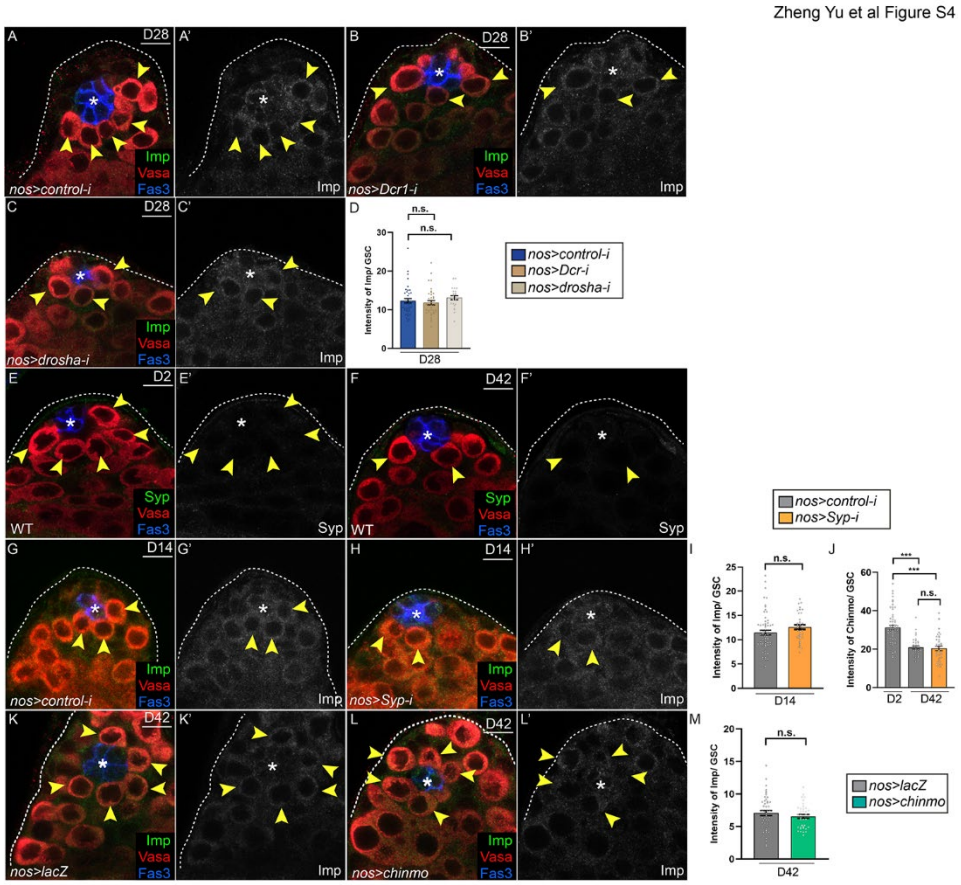

Figure S4. Imp is not regulated by miRNAs, Syp, or Chinmo in GSCs, related to Fig. 4

(A–D) Confocal images of Imp protein (green) in D28 *nos>control-i* (A) or *nos>Dcr-1-i* (B) or *nos>drosha-i* (C) testes, quantified in D. Arrowheads indicate Imp expression in GSCs.

(E, F) Confocal images of Syp protein (green) in D2 (E) or D42 (F) testes. Arrowheads mark GSCs.

(G-J) Confocal images of Imp protein (green) in D14 *nos>control-i* (G) or *nos>syp-i* (H) testes, quantified in I. Arrowheads indicate Imp expression in GSCs. Graph (J) showing Chinmo protein expression in D2 or D42 *nos>control-i* (gray bars) and D42 *nos>syp-i* (orange bars) testes.

(K-M) Confocal images of Imp protein (green) in D42 testes of *nos>control-i* (K) or *nos>chinmo* (L) testes, quantified in M. Arrowheads mark Imp expression in GSCs. Asterisks indicate niche cells. Vasa marks germ cells and Fas3 labels niche cells.

Scale bars = 10 μm.

Error bars in I, J, M represent SEM. *** $P \leq 0.001$; n.s. indicates no significance, as determined by Student's t-test (see STAR Methods).

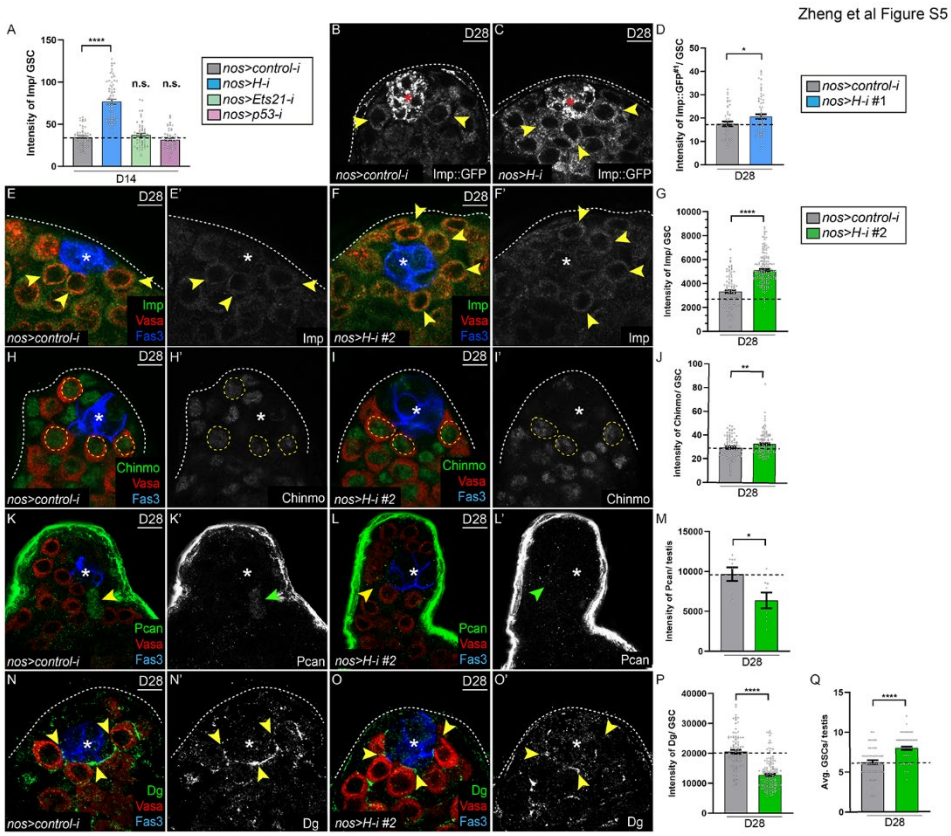

Figure S5. Hairless represses Imp protein in GSCs, related to Fig. 5

(A) Graph showing the intensity of Imp protein in D14 *nos>control-i* (gray bar), *nos>H-i* (blue bar), *nos>Ets21-i* (green bar), or *nos>p53-i* (purple bar) testes.

(B–D) Confocal images of Imp::GFP (gray) in D28 *nos>control-i* (B) or *nos>H-i* (C) testes, quantified in D. Arrowheads indicate Imp::GFP expression in GSCs.

(E–G) Confocal images of Imp protein (green) in D28 *nos>control-i* (E) or *nos>H-i#2* (F) testes, quantified in G. Arrowheads mark Imp in GSCs.

(H–J) Confocal images of Chinmo protein (green) in D28 *nos>control-i* (H) or *nos>H-i#2* (I) testes, quantified in J. Dashed lines indicate GSCs.

(K–M) Confocal images of Pcan protein (green) in D28 *nos>control-i* (K) or *nos>H-i#2* (L) testes, quantified in M. Arrowhead indicates ectopic Pcan surrounding the niche.

(N–P) Confocal images of Dg (green) at the GSC–niche interface in D28 *nos>control-i* (N) or *nos>H-i#2* (O) testes, quantified in P. Arrowheads mark Dg at the GSC–niche interface.

(Q) Graph of the total number of GSCs in D28 *nos>control-i* (gray bar) or *nos>H-i#2* (green bar) testes.

Asterisks indicate niche cells. Vasa marks germ cells and Fas3 labels niche cells.

Scale bars = 10 μm.

Error bars in A, D, G, J, M, P, Q represent SEM. * $P \leq 0.05$; ** $P \leq 0.01$; **** $P \leq 0.0001$ by Student's t-test (see STAR Methods).

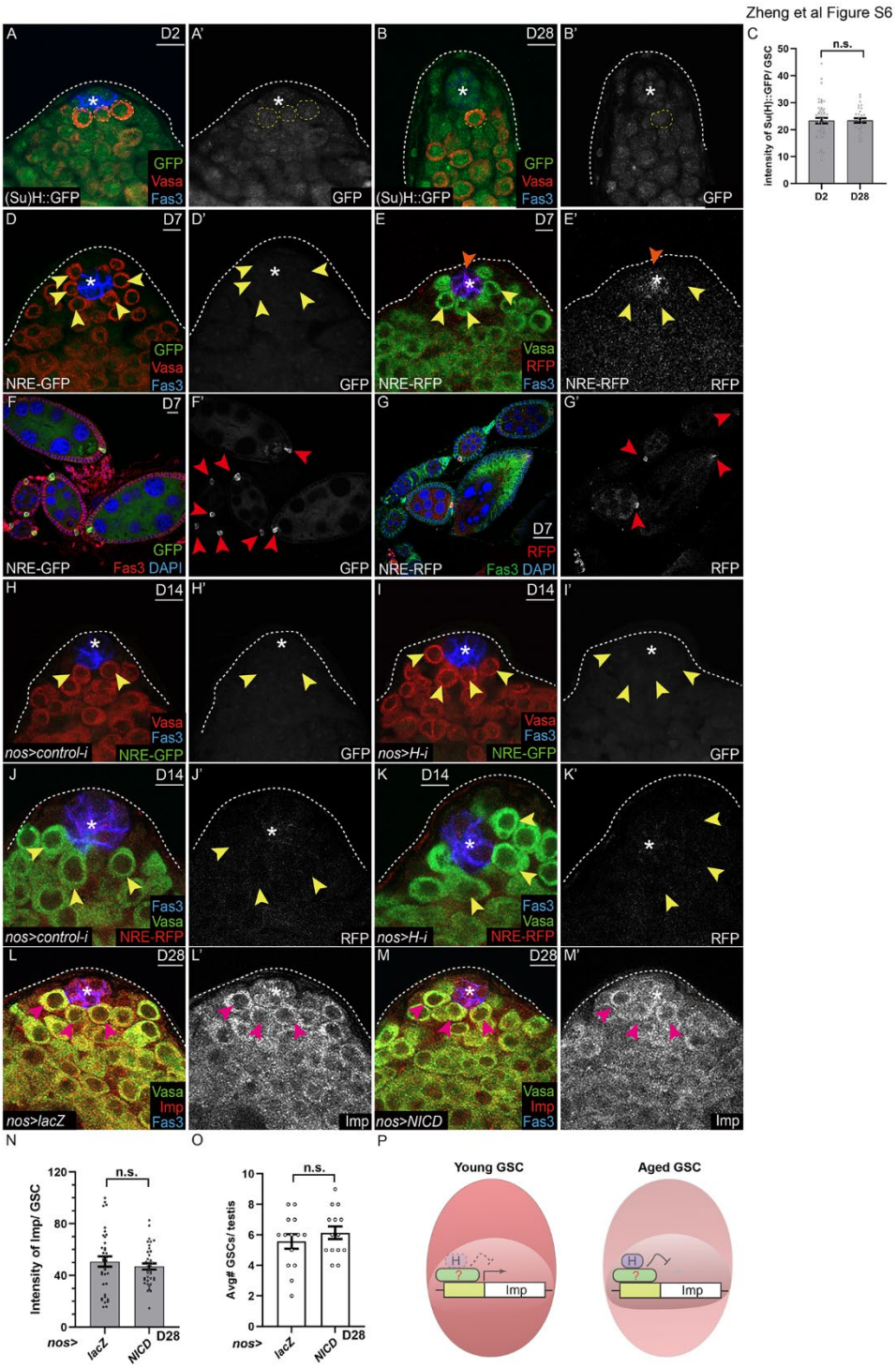

Figure S6. Notch signaling is not observed in adult testes, related to Fig. 5

(A-C) Confocal images of Suppressor of Hairless::GFP ((Su)H::GFP) (green) in D2 (A) or D28 (B) testes, quantified in C. Dashed lines indicate GSCs.

(D-G) Confocal images of NRE-GFP (D, F) and NRE-RFP (E, G) in D7 testes (E, F) or in D7 ovaries (F, G). Yellow arrowheads indicate GSCs (D, E), while the orange arrowhead (E)

indicates NRE-RFP expression in niche cells. Arrowheads in F, G indicate ovarian polar cells that express NRE-GFP (F) or NRE-RFP (G) reporters.

(H-K) Confocal images of NRE-GFP (H, I) and NRE-RFP (J, K) in D14 *nos>control-i* (H, J) or *nos>H-i* (I, K) testes. Arrowheads indicate GSCs.

(L-O) Confocal images of Imp protein (red) in D28 *nos>lacZ* (L) or *nos>NICD* (M) testes, quantified in N. Arrowheads indicate GSCs. Graph in O showing the average number of GSCs in D28 *nos>lacZ* or *nos>NICD* testes.

(P) Model of H repression of *Imp*. H interacts with an as-yet unknown protein (green shape with question mark) to repress *Imp* gene expression. In young GSCs (left), H (shape outlined with dashed line) is low, permitting robust *Imp* gene expression. At later adult stages (right), H (purple box) increases, leading to repression of the *Imp* gene. H-mediated repression of *Imp* occurs independently of H's canonical role in the Notch pathway.

Asterisks indicate niche cells. Vasa marks germ cells and Fas3 labels niche cells except for G and H, where Fas3 marks ovarian follicle cells.

Scale bar = 10 μM

Error bars in C, N, O represent SEM. n.s. indicates no significance as assessed by Student's t-test (see STAR Methods).

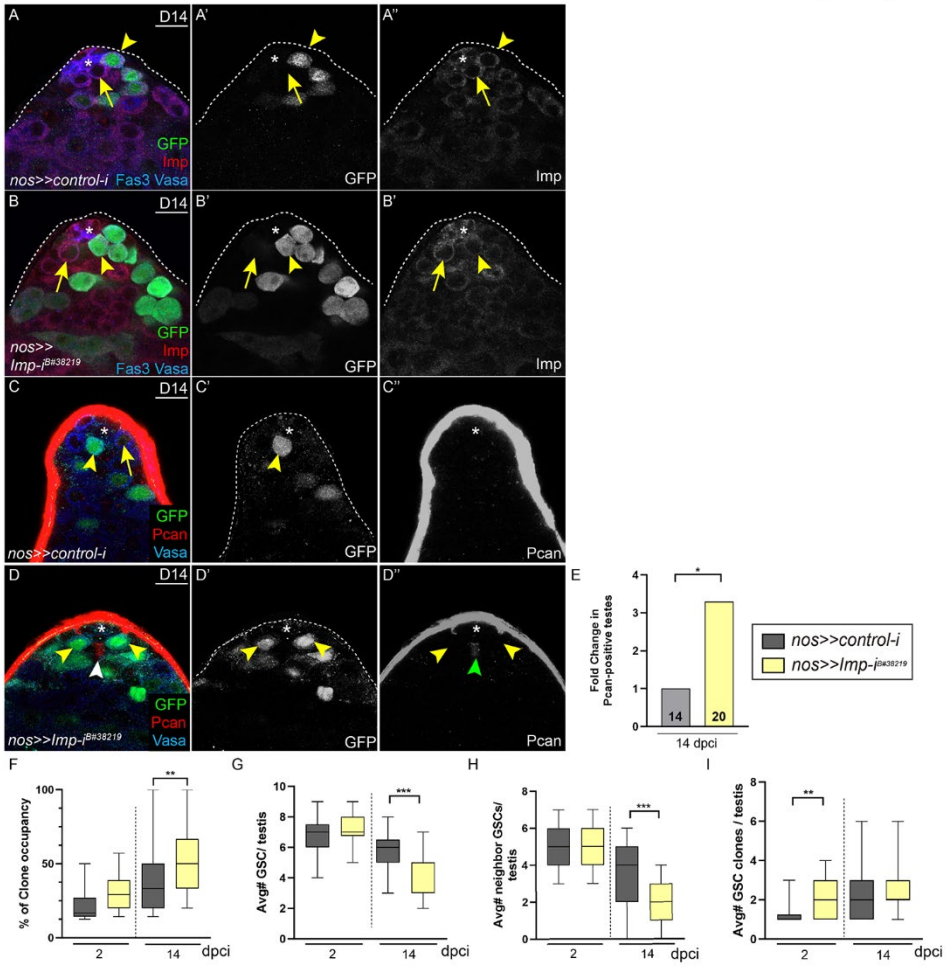

Figure S7. *Imp*-mutant GSCs are more competitive, causing niche remodeling, and evicting non-mutant GSC neighbors, related to Fig. 7

(A-B) Confocal image of Imp protein (red) in testes with *nos>>control-i* GSC clones (A) or *nos>>Imp-i* GSC clones (B) at 14 dpci. Arrowheads indicate the GFP-positive GSC clone. Arrows indicate non-mutant neighboring GSCs.

(C-E) Confocal image of Pcan protein (red) in the testis with *nos>>control-i* GSC clones (C) or *nos>>Imp-i* GSC clones (D) at 14 dpci. Arrowheads indicate GFP-positive GSC clones. Magenta arrowhead indicates ectopic Pcan deposition around the niche in testes with *nos>>Imp-i* GSC clones, quantified in E. Sample size for each genotype is indicated in the bar.

(F-I) Box and whisker plots showing clone occupancy (F), average total number of GSCs (G), average number of non-mutant GSC neighbors (H), and average number of GSC clones (I) in testes with control *nos>>control-i* GSC clones (gray bars) or *nos>>Imp-i* GSC clones (yellow bars) at 2 and 14 dpci.

Asterisks indicated niche cells. Vasa marks germ cells and Fas3 labels niche cells.

Scale bar = 10 μM

In G-I, error bars represent SEM. * $P \leq 0.05$; ** $P \leq 0.01$; *** $P \leq 0.001$ as assessed by Student's t-test for F-I and by χ^2 test for E (see STAR Methods).